Available online at www.sciencedirect.com

ScienceDirect

Geochimica et Cosmochimica Acta xxx (2013) xxx–xxx

Geochimica et Cosmochimica Acta

www.elsevier.com/locate/gca

Speleothem trace element signatures: A hydrologic geochemical study of modern cave dripwaters and farmed calcite

Darrel M. Tremaine [a,*], Philip N. Froelich [b]

[a] Department of Earth Ocean and Atmospheric Science, National High Magnetic Field Laboratory, Florida State University, 1800 E. Paul Dirac Drive, Tallahassee, FL 32310-3706, United States

[b] Froelich Education Services, 3402 Cameron Chase Drive, Tallahassee, FL 32309-2898, United States

Received 18 November 2012; accepted in revised form 21 July 2013; available online xxxx

Abstract

Trace element variations in ancient cave speleothems are often interpreted as indicators of changes in paleo-rainfall and hydrologic conditions. However, these records are difficult to interpret without an understanding of the physicochemical controls on stalagmite chemistry plus site-specific calibration of changes in *net* rainfall to variations in dripwater and speleothem chemistry. In this study we examine geochemical relationships between *net* rainfall (Precipitation minus Evapotranspiration; P−ET), drip rates, drip water chemistry, and contemporaneous calcite chemistry to test the hypothesis that speleothem Mg/Ca and Sr/Ca records are proxies for rainfall amount.

HRC is contained within four low-magnesium limestone units capped sporadically by a remnant dolomitic limestone. Aqueous concentrations of magnesium (post evapotranspiration) decrease with increasing vertical travel distance between the soil zone and the point of in-cave drip emergence (*Drip Path Length* – DPL) as dissolved high-Mg solutions sourced from the dolomitic caprock are diluted with dissolved low-Mg limestone waters sourced from the host limestone. Dripwater Mg/Ca and Sr/Ca ratios covary and provide diagnostic indicators of the two dominant mechanisms controlling dripwater chemistry: (1) mixing of post-evaporative solutions derived from two geochemical endmembers (dissolution of dolomite and limestone); and (2) evolution of hydrochemistry away from dissolved bedrock compositions due to Prior Calcite Precipitation (PCP) above the drip sites. By resolving the linear mixing relationships for drip water Mg/Ca and Sr/Ca sources and the distribution coefficients for trace element transfer in the PCP dripwater-to-calcite precipitation reactions and applying these principles to our time series, we find that the extent of PCP production within the karst is directly controlled by the balance between Precipitation (P) and Evapotranspiration (ET): higher *net* rainfall (P−ET > 1: wet conditions) reduces PCP, and lower *net* rainfall with increased evapotranspiration (P−ET < 1) increases PCP.

Farmed calcite X/Ca ratios faithfully track hydrologically-influenced seasonal variations in dripwater chemistry for X = Mg, Sr, and Na. However, the relationship between changes in *net* rainfall and changes in Mg/Ca and Sr/Ca ratios in modern calcite is unique at each site and differs significantly at closely-spaced drip/stalagmite locations. This suggests that *in situ* modern hydrochemical calibrations should be performed atop individual speleothems prior to harvesting for paleoclimate investigations, and that such calibrations may not reflect past conditions as drip paths change. We apply this understanding to published dripwater data and speleothem time series from other caves. A major implication is that in order to interpret stalagmite Sr/Ca and Mg/Ca ratios as 'wet vs. dry' proxies, speleothem Sr/Ca and Mg/Ca variations must be coherent and in-phase over all time periods (i.e., Sr/Mg ratios must be constant). These criteria will help to distinguish 'rainfall amount' versus 'rainfall source' in speleothem $\delta^{18}O$ records.

1. INTRODUCTION

Cave formations, or speleothems, are valuable archives

* Corresponding author. Tel.: +1 513 315 2583.
E-mail address: tremaine@magnet.fsu.edu (D.M. Tremaine).

0016-7037/$ - see front matter © 2013 Elsevier Ltd. All rights reserved.
http://dx.doi.org/10.1016/j.gca.2013.07.026

of paleoclimate information because they preserve fluctuations in stable isotopic compositions and trace element chemistries of their formation waters (Holland et al., 1964a; Hendy, 1971; Gascoyne, 1983). Speleothem oxygen isotopes ($\delta^{18}O$) have long been used to reconstruct regional rainfall source and amount variations (Bar-Matthews et al., 1996; Burns et al., 2001; Wang et al., 2008). However, water vapor sources and rainfall amount are often difficult to separate, a problem that has led to investigations of additional speleothem-based hydrologic proxies such as growth rates, annual banding thickness, crystal habit, humin content, and trace element compositions (Broecker et al., 1960; Baker et al., 1993, 1997; Fairchild et al., 2000; Frisia et al., 2000; Polyak and Asmerom, 2001; Baldini et al., 2002; Treble et al., 2003; Johnson et al., 2006; Borsato et al., 2007; Cruz et al., 2007; Tremaine, 2010).

Seasonal (cyclical) variations in Mg/Ca and Sr/Ca have been measured in dripwaters inside many caves throughout Europe and UK (Baker et al., 2000; Fairchild et al., 2000, 2006; Spötl et al., 2005; Baldini et al., 2006, 2012; Verheyden et al., 2008; Riechelmann et al., 2011)), USA (Musgrove and Banner, 2004; Tremaine, 2010; Wong et al., 2011; Oster et al., 2012), Australia (McDonald and Drysdale, 2004; McDonald et al., 2007), and Brazil (Karmann et al., 2007). Fluctuations in element to calcium ratios (X/Ca) have been observed in speleothems on millennial timescales (Goede and Vogel, 1991; Ayalon et al., 1999; Bar-Matthews et al., 1999; Hellstrom and McCulloch, 2000; Verheyden et al., 2000; Li et al., 2005; Cruz et al., 2007) and on decadal to seasonal timescales (Goede et al., 1998; Roberts et al., 1998, 1999; Fairchild et al., 2001; Huang et al., 2001; Baldini et al., 2002; Finch et al., 2003; Treble et al., 2003, 2005; McMillan et al., 2005; Desmarchelier et al., 2006; Johnson et al., 2006; Borsato et al., 2007; Griffiths et al., 2010; Jo et al., 2010).

The current hydrochemical paradigm commonly invoked to explain variations in stalagmite chemistry holds that drier conditions (less rainfall, more evapotranspiration) promote longer water residence times in the epikarst, decreased drip rates, and enhanced CO_2 degasing into air voids within the unwetted epikarst, a form of ventilation. These conditions lead to Mg/Ca and Sr/Ca ratios higher than congruent limestone dissolution due to preferential removal of Ca (discrimination against Mg and Sr) during diagenetic calcite deposition upstream from the stalagmite, known as Prior Calcite Precipitation (PCP) (Fairchild et al., 2000). PCP can occur in the overlying regolith or on the cave ceiling, walls, flowstone, stalactites, or soda straws above the dripwater collection site. Conversely, wetter conditions (more rainfall, less evapotranspiration) are thought to promote higher hydraulic head, faster drip response times, reduced water residence times, slower CO_2 degasing, and lower Mg/Ca and Sr/Ca ratios due to reduced PCP and enhanced limestone dissolution (Fairchild et al., 2000; Treble et al., 2003; Johnson et al., 2006; Cruz et al., 2007). Once the aquatic soil and epikarst system has come to saturation with respect to calcite by limestone dissolution in very high pCO_2 (soil gas) conditions, any ventilation that subsequently removes CO_2, whether via aeration of soils or epikarst, or inside caves that are breathing (Kowalczk and Froelich, 2010), promotes PCP-calcite precipitation along flow and drip pathways.

Although variations in elemental compositions of calcite dripstones have evoked a variety of interpretations, they are seldom calibrated in present-day conditions to provide *quantitative* paleoclimate proxies. The purpose of this paper is to demonstrate a method to quantify modern calcite trace element changes related to contemporaneous hydrologic variations, complementing our previous isotopic calibrations of modern calcite $\delta^{18}O$ and $\delta^{13}C$ for both *in situ* cave temperature and cave air ventilation (Kowalczk and Froelich, 2010; Tremaine et al., 2011). Here we link local climatology and cave dripwater chemistry to contemporaneous calcite chemistry from semi-continuous snapshots at several drip sites inside one shallow Florida cave, and then interpret the relationships with respect to modern rainfall and *in situ* drip rate conditions. Our HRC dripwater-calcite Sr/Mg calibrations are then tested with other cave dripwater data sets and speleothem records to judge general applicability over a range of different cave conditions.

1.1. Distribution coefficients

Cave dripwaters often exhibit drip rate and drip chemistry variations between drip sites in response to changing rainfall recharge and dripwater flow paths through the bedrock (Smart and Friedrich, 1986; Genty and Deflandre, 1998; Baker et al., 2000; Tooth and Fairchild, 2003; Baldini et al., 2006). These chemical fluctuations may then be imparted to speleothem calcite and preserved as an indicator of contemporaneous hydrologic activity. Laboratory-based inorganic calcite precipitation experiments similar to natural cave precipitates have been performed under well-controlled solution chemistry conditions to determine trace element partitioning into calcite (Kitano et al., 1971; Katz et al., 1972; Lorens, 1981; Huang and Fairchild, 2001; Gabitov and Watson, 2006, and others). Huang and Fairchild (2001) examined trace elements under variable but controlled $[Ca^{2+}]$, $[HCO_3^-]$, and pCO_2 conditions that closely mimicked natural cave systematics. Despite this multitude of laboratory studies, proxy calibrations of trace element compositions based on modern natural speleothem calcite farmed under active drips in natural cave systems are rare (see Holland et al., 1964a; Gascoyne, 1983; Huang et al., 2001; Stern et al., 2005; Guilfoyle, 2006).

A first step toward calibrating modern calcite chemistry to drip chemistry is to establish field-based H_2O–$CaCO_3$ distribution coefficients $[D_X]$ analogous to the lab-based work (Henderson and Kraček, 1927; McIntire, 1963; Morse and Bender, 1990):

$$D_X = \frac{(X/Ca)_{CaCO_3}}{(X/Ca)_{Aq}}$$

where X is the concentration of the cation of interest. A number of laboratory and cave studies have demonstrated a temperature dependence on D_{Mg} (Katz, 1973; Gascoyne, 1983; Mucci and Morse, 1990; Huang and Fairchild, 2001). Others have reported growth rate dependencies on D_{Na}, D_{Sr}, and D_{Ba} in both laboratory calcite and in speleothems (Lorens, 1978, 1981; Mucci and Morse, 1983; Ishikawa and

Ichikuni, 1984; Tesoriero and Pankow, 1996; Huang and Fairchild, 2001; Treble et al., 2003, 2005; Gabitov and Watson, 2006). In Section 4.5 we develop D_X for several elements, and then in Section 5 we apply these to dripwater and calcite precipitates. We examine partitioning at multiple drip sites in a single cave to enable 'unmixing' of the geochemical sources and processes leading to changes in both drip and calcite chemistry.

1.2. Hydrologic controls on dripwater chemistry

It has long been recognized that bedrock and dripwater chemistry are primary controls on speleothem chemistry (Holland et al., 1964a; Hendy, 1971; Gascoyne, 1983; Banner, 1995). Early work with ultraviolet fluorescence revealed light and dark annual banding in stalagmites (Baker et al., 1993). These color laminae were attributed to fulvic and humic acid content that peaked with autumnal rainfall. Corresponding seasonal variations were later observed in stalagmite Mg/Ca, Sr/Ca and Ba/Ca ratios (Roberts et al., 1998) which were thought to be hydrologically modulated. In addition to hydrologic controls, crystallography has also been invoked to describe micro-scale factors such as crystal cleavage and fractures, annual dissolution horizons, growth hiatuses, incongruent weathering of carbonate sources, enhanced dissolution of dolomite, and selective leaching of Mg and Sr from non-carbonate minerals (Busenberg and Plummer, 1982; McGillen and Fairchild, 2005; Desmarchelier et al., 2006). Although fluctuations in speleothem chemistry are often inferred to be caused by concentration changes in source water, contemporaneous dripwater and speleothem chemistry data are generally lacking. As a result, hydrochemical constraints on speleothem chemistry are not well established (Roberts et al., 1998, 1999; Finch et al., 2003; Treble et al., 2003; Li et al., 2005; Smith et al., 2009; Griffiths et al., 2010).

Roberts et al. (1999) has argued that three coeval stalagmite Sr/Ca and Mg/Ca time series records from one cave, Goddard-Barker "GB" Cave (England), did not match each other in phase or magnitude. They implied that the Sr/Mg ratio could not be used as a tool for quantitative paleotemperature reconstructions as had been suggested by Gascoyne (1983) and Goede and Vogel (1991). These findings further underscored the original assertion of Roberts et al. (1998) that "*trace element partitioning at the water–calcite interface cannot be investigated in isolation from the remainder of the hydrochemical system*" but must be examined with some understanding of the processes controlling dripwater geochemistry.

2. STUDY SITE

Hollow Ridge Cave (HRC) is a shallow phreatic-zone cave in Marianna, Florida, formed within a 15-m thick limestone knoll comprised of the flat-lying Marianna, Bumpnose, and Ocala members of the Oligocene-aged (38–35 Ma) Ocala limestone formation, capped by sporadic remnants of dolomitic limestone (Scott, 1991, 2001; Green et al., 2003; Kowalczk, 2009). There are over 1030 m of mapped passage within HRC (Fig. EA.1), composed of southeast-to-northwest trending vertical passages (4–8 m tall) typical of the regional fault structure, connected by low east–west tunnels (1.5 m tall) within the more friable Bumpnose formation. The maximum and minimum overhead limestone thicknesses are approximately 10 m (Ballroom) and 1 m (Signature Room) (Tremaine, 2010). HRC has four known entrances: three at the west end adjacent to the floodplain of the Chipola River (21 m above sea level) (Ent. A, B and C; Fig. EA.1), and one on the south side elevated in the bluff (28 m above sea level) (Ent. D; Fig. EA.1). The cave is overlain by a thin, poorly developed, and well drained soil layer (average < 30 cm thick) composed of Plio-Pleistocene sands and clays with numerous bedrock outcrops (Maddox, 1993). The vegetation is characterized as an upland mixed forest, composed primarily of C3 trees (mostly slash pine) and C4 shrubs and vines. Slash pine trees have taproots that penetrate downward into bedrock, and tree roots are visible at several locations inside the cave. See Kowalczk (2009) and Tremaine (2010) for more detailed descriptions.

Subtropical Marianna, Florida normally receives rainfall all year long, so that the amplitude of seasonal aqueous trace element variations is not pronounced. About $80 \pm 7\%$ of the rainfall in this region is evaporated, which is typical for pine flat-wood ecosystems in the subtropics (Bidlake et al., 1996). Mean annual precipitation in Quincy, Florida (71 km east of Marianna, Florida) is approximately 1377 mm yr^{-1} (1984–2010; www.ncdc.noaa.gov) or about 115 mm $month^{-1}$. Total mean monthly *gross* rainfall at HRC during this study was 118 ± 58 mm $month^{-1}$ (2007–2010), near the 25-year average. Mean annual outside air temperature measured above HRC (2007–2010) was 18.3 °C, and mean monthly temperatures range from 8.6 °C (January 2008) to 26.6 °C (June 2009). Mean annual cave air temperatures at Cave Station 1 (CS1) and Cave Station 2 (CS2) were 18.8 °C (ranging from 12.6 to 23.9), and 19.5 °C (ranging from 17.7 to 22.9), respectively. Cave Station 1 is near the cave entrances and thus subject to atmospheric ventilation while Cave Station 2 is in the deep interior of the cave where air temperature reflects mean annual bedrock temperature (Kowalczk and Froelich, 2010). This temperature range is not typical of deep caves and is discussed at length by Tremaine et al. (2011).

3. MATERIALS AND METHODS

Ballroom drip rates were continuously monitored from June 2008 through February 2010 using a Stalagmate MK2 Plus acoustic drip recorder (Collister and Mattey, 2005) at the point of maximum overhead epikarst thickness to monitor seepage-flow response to rainfall recharge (see Figs. 1 and EA.1 for locations and EA.3 for flow characteristics). Drip rate snapshots were obtained monthly using a stopwatch at all other sites during dripwater collection. Hourly drip rates are converted to volumetric flow rates (mL min^{-1}) using 0.12 mL $drip^{-1}$ measured from stalactite tips (Tremaine, 2010). Brief hiatuses in data collection occurred during three floodwater inundations (Kowalczk, 2009; Tremaine, 2010). Ballroom and Sump (groundwater)

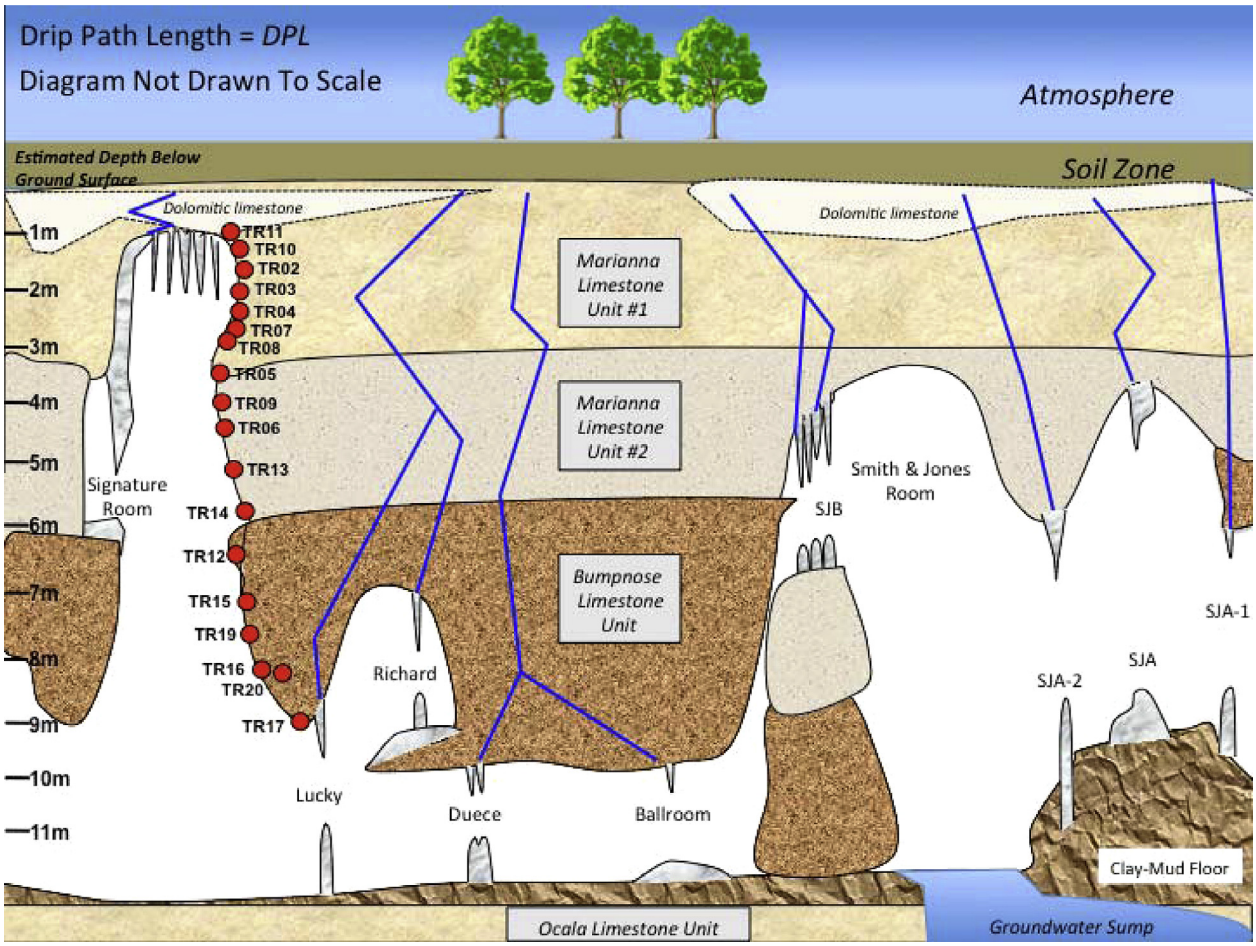

Fig. 1. Conceptual vertical stratigraphic cross section of HRC drip water flow paths. Relative thickness of each layer is estimated from vertical surveys, and the location of each dolomitized limestone rind is inferential (dashed lines). Blue lines represent idealized drip water flow paths through the epikarst, which are likely to be much more convoluted than shown here. Vertical drip path length (DPL) above each calcite farming location can be estimated from the scale on the left side of the figure. Red circles denote vertical wall-rock transect sampling locations (data shown in Tables 2, EA.3, and EC.5). (For interpretation of the references to color in this figure legend, the reader is referred to the web version of this article.)

samples were collected bi-weekly from June 2008 through February 2010. Smith and Jones Room A (SJA) and Smith and Jones Room B (SJB) samples were collected bi-weekly from June 2009 through February 2010. Duece samples were collected bi-weekly between October 2009 and February 2010. Signature Room samples were sporadically collected directly following large rainfall events. Weekly rainfall cation and anion concentrations for nearby Quincy, Florida (71 km east of HRC) were provided by the National Atmospheric Deposition Program from 12/25/07 to 2/23/10 (http://nadp.sws.uiuc.edu), and for Pensacola, Florida (216 km southwest of HRC) by William Landing (Florida State University) from 6/11/08 to 9/20/09 (see Landing et al., 2010).

Rainfall precipitation (P) was measured directly atop HRC. Monthlyevapotranspiration (ET) was estimated using the "Thornthwaite" equations after Willmot et al. (1985) (see calculations in Table EA.1). Monthly *net* rainfall (P−ET) was calculated as the difference between the two parameters. It should be noted that this approach likely under-estimates actual infiltration into the cave because the northern Gulf of Mexico (NGOM) region is recharged by heavy precipitation events that overwhelm ET on short timescales.

Chloride and sulfate concentrations in cave dripwaters were measured from undiluted samples on a Dionex 4500i Ion Chromatograph. Calibrations were performed at the beginning, middle, and end of each run using in-house IC check standards prepared from *Ultra Scientific*™ primary standards. Analytical uncertainties (1σ) for each sample were ± 0.95 μmol L^{-1} for $[Cl^-]$ and ± 0.25 μmol L^{-1} for $[SO_4^{2-}]$. Data are presented in Table EC.3.

Unfiltered major cation and trace element samples were diluted to approximately 1 ppm [Ca] by adding 30 μL sample to 3.95 mL 2% *Optima*™ HNO_3 and spiked to 10 ppb Sc, In, and Y (internal standards). Samples were then measured for Li, Na, Si, Mg, K, Ca, Mn, and Sr on an *Agilent*™ 7500cs Quadrupole ICP-MS following multiple-element standard-bracketing methods (modified after Yu et al.,

2005). Calibrations were performed approximately every ten samples using matrix-matched standards created from gravimetrically prepared serial dilutions of *Specpure*™ standards. Analytical uncertainties (1σ) were less than ± 0.05 μmol L^{-1}.

In November 2008 calcite farming was initiated on 2.5×7.5 cm glass microscope slides placed under eleven active drip sites (Fig. EA. 1). Before deployment, slides were pre-weighed and then fixed tilted with a flexible wire mesh atop actively growing (dripping) stalagmites similar to the methods of Frisia et al. (2000), Mickler et al. (2004), Banner et al. (2007), and Boch et al. (2009). After visual verification of calcite growth, slides were removed and replaced seasonally, approximately every three months. Recovered slides were rinsed with deionized water to remove residual salts, then dried and weighed. Low-magnesium calcite growth was verified using visual microscopy of crystal habit and X-ray Diffraction. No aragonite or vaterite was observed (Tremaine, 2010). After weighing, 30–200 μg of calcite was selectively removed from each glass plate, dissolved in 100 μL of 7 N HNO_3, then diluted with 18 MΩ deionized water to ~1 ppm [Ca] and analyzed on an *Agilent*™ 7500cs Quadrupole ICP-MS following the dripwater protocols. Each plate was previously sampled for isotopes and ^{14}C, thus trace element samples were taken from random spots on each plate. Even though most plates were covered with a thin film of crystals, this heterogeneous sampling routine probably introduces uncertainty in distribution coefficients due to spatially variable crystal composition (Mickler et al., 2006; Day and Henderson, 2011).

Fig. 1 depicts an idealized vertical section through HRC with surveyed estimates of the water travel distance from ground surface through the epikarst to the point of drip emergence at each drip site (referred to as *Drip Path Length* or *DPL*). Eighteen wall-rock limestone samples were collected in a vertical profile inside the cave, starting at the ceiling at the east end of the Fissure Crack (approximately 0.6 m below ground surface – Fig. 1) and ending at the ceiling of the base level of the cave 9.2 m below ground surface. Recrystallized wall-rock rind was removed at each location and fresh limestone was collected into pre-cleaned polyethylene bottles. All limestone samples were analyzed via X-ray Diffraction at MARTECH, Dept. of Physics, Florida State University. Three soil samples were also collected from above HRC near the MET station, above SJB, and above the Ballroom. Soil and bedrock samples were dried for 48 h in glass vials and then individually homogenized using an aluminum oxide mortar and pestle. Three to five subsamples were weighed from each vial (30–300 μg each) and then dissolved into 100 μL of 7 N *Optima*™ HNO_3. After centrifuging and passing through a 0.45 μm filter, samples were diluted to 0.5 ppm [Ca] in 2% *Optima*™ HNO_3 and analyzed on an *Agilent*™ 7500cs Quadrupole ICP-MS following the dripwater protocols. Analytical uncertainties (1σ, $n = 5$) calculated for each sample were ± 2.4 mmol mol^{-1} for Mg/Ca and ± 0.39 mmol mol^{-1} for Sr/Ca. Data are presented in Table EC.5.

In order to establish geochemical constraints for speleothem paleohydrologic proxy X/Ca interpretations, it is useful to determine solution-calcite distribution coefficients and compare them with lab calcite experiments and with other cave studies. To calculate D_X, averaged X/Ca ratios in HRC dripwaters were compared to X/Ca ratios in modern farmed calcite during each seasonal farming period (Table EC.1). Distribution coefficients were then compared among individual drip sites to assess their uniformity throughout the cave.

4. RESULTS

4.1. *Net* rainfall amount and drip rate

A step toward understanding hydrologic controls of dripwater and calcite compositions at HRC is establishing how fluctuations in *net* rainfall amount (Precipitation minus Evapotranspiration: P−ET) affect dripwater response times and drip rates. Evapotranspiration removes water from the soil, concentrating ions in soil water by up to a factor of eighteen (~93% ET). Florida experienced drought conditions from March through November 2008, creating generally negative *net* rainfall at HRC with maximum monthly water deficits of −121 mm (May) and −115 mm (September). Average *net* rainfall during this pronounced 9-month dry period was −27 mm $month^{-1}$ and ET was approximately 90.3% (Fig. 2a) (see P−ET calculations in Table EA.1). During July 2008 high evapotranspiration and reduced rainfall resulted in the driest *in situ* conditions of the study period (drip rate ~0.06 mL min^{-1}) (Fig. 2b – Marker 'A'). A cold front delivered 70 mm of rainfall on August 15th, 2008 and Tropical Storm Fay delivered 118 mm of rainfall on August 22nd, 2008. These two events recharged the epikarst at HRC and increased the Ballroom drip rate to 2.6 mL min^{-1} after a lag time of approximately 14 days (Kowalczk, 2009).

The epikarst remained hydrologically saturated (full-pool) through September 2008 as indicated by a sustained maximum Ballroom drip rate resulting from piston flow, likely through cracks and fissures. After the cracks and fissures emptied, the piston flow was exhausted and porous flow became the dominant flow regime, resulting in an instantaneous 0.15 mL min^{-1} reduction in flow rate on October 10th. A linear fall-off in drip rate began on October 10th and continued through December 12th, after which flooding rains again recharged the epikarst to maximum capacity. During the subsequent 6-month wet period (December 2008–May 2009) average *net* rainfall was +22 mm $month^{-1}$ and ET was approximately 77.6%. After each month of positive*net* rainfall (e.g., August and December, 2008) sustained increases in drip flow volumes were recorded. This pattern of epikarst recharge to full-pool (piston flow) followed by a small instantaneous flow reduction and subsequent linear drip rate fall-off was observed over six intervals (marked I to VI in Figs. 2b and 3).

Linear drip loss rates (L) were calculated for each episode (periods I through VI in Fig. 2b). Linear drip loss rates ranged from $L = -2.6 \times 10^{-3}$ mL min^{-1} hr^{-1} to $L = -0.8 \times 10^{-3}$ mL min^{-1} hr^{-1}. Loss rates are similar to within a factor of two for all events. Water flow halving-times (time required for drip flow rates to decrease by half)

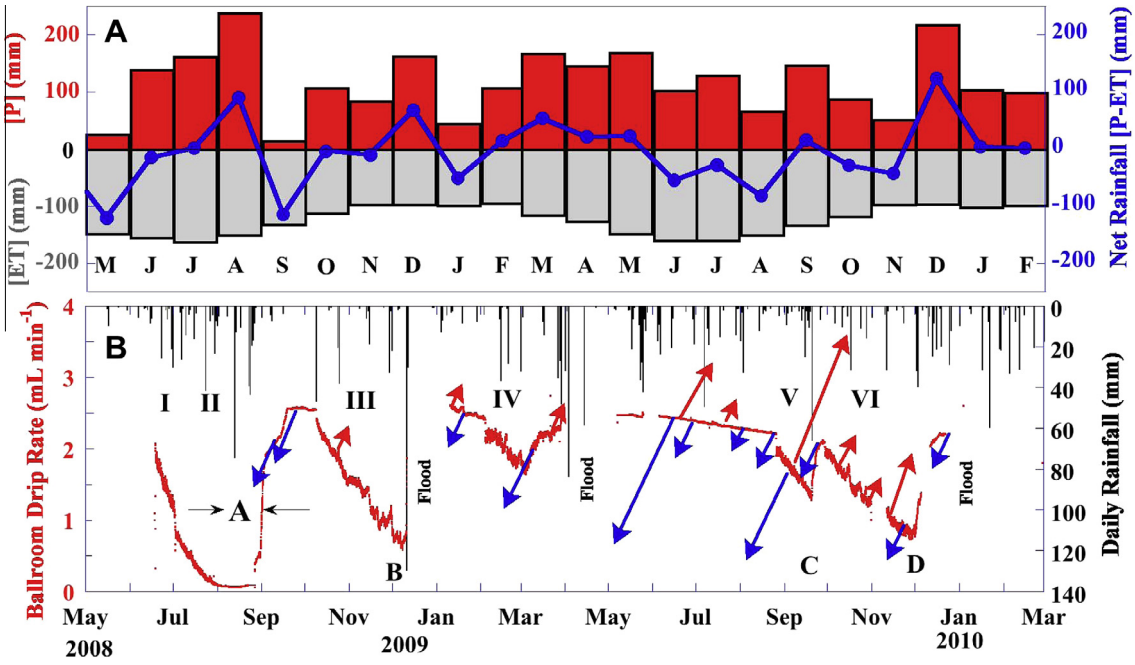

Fig. 2. (Panel A) Left Y-axis: Monthly precipitation above HRC denoted as [P] (red bars) and monthly evapotranspiration as [ET] (grey bars). Right Y-Axis: Monthly *net* rainfall [P−ET] (blue circles and solid blue lines). Data and calculations are presented in the Electronic Annex (Table EA.1). (Panel B) Left Y-axis: Ballroom drip rate (red points). Right Y-axis: Daily rainfall above HRC (hanging black bars). Missing drip rate data are periods when the drip logger was displaced by flood events (e.g., December 16th 2008 through January 10th 2009). Event 'A' and bracketing arrows illustrate the 14-day (or longer) lag time between a heavy rain event and the rapid drip rate response after a dry period of empty epikarst reservoir pool with a long water response time. Markers B, C, and D illustrate a greatly reduced lag time in drip rate response to rainfall during periods of filling or full epikarst. Periods of drip rate decrease during falling reservoir volume are marked with Roman numerals I through VI and are expanded in Fig. 3. See Section 5.1.2: Diagonal arrows represent changes in dripwater Sr/Ca and Mg/Ca ratios taken from the PCP vectors in Fig. 6. The length of the arrow denotes the magnitude of PCP change ($\Delta Sr/\Delta Mg$), and the arrow origins (tails) designate the end-of-event date. Arrow lengths were generated by plotting change in PCP along the Ballroom PCP vector in Fig. 6b and then translating to Fig. 2 (plots not shown here). Blue arrows pointing toward the lower left indicate reduced dripwater Sr/Ca and Mg/Ca ratios (toward the origin in Fig. 6), reduced extent of PCP, and should correlate with wet conditions and increasing or high drip rates. Red arrows pointing toward the upper right indicate increased dripwater Sr/Ca and Mg/Ca ratios (away from origin in Fig. 6), increased extent of PCP, and should correlate with dry conditions and decreasing or low drip rates. This pattern of increased Sr/Ca and Mg/Ca (dry) versus decreased Sr/Ca and Mg/Ca (wet) is observed during periods of significant drip rate fluctuation (e.g., June 2008 through December, 2008; September 2009 through January 2010). However, between March 2009 and September 2009 when Ballroom drip rates exhibit a sustained drip rate 'high' there is no clear relationship between drip rate and changes in Sr/Ca or Mg/Ca ratios.

ranged from 2.1 to 6.7 weeks (Fig. 3). Halving-times are shorter during periods of lower net rainfall (2008; long water response times), and longer during periods of higher net rainfall (2009; short water response times). This drip rate behavior provides information on the hydraulic response time of the water in the epikarst as it penetrates downward through the system, a reliable indicator of periods when the epikarst is full (and likely overflowing), and when it is dry.

A saw-tooth pattern is observed in expanded views of each drip rate fall-off (Fig. 3, panel VII). These semi-diurnal drip cycles are directly related to changes in barometric pressure caused by the diurnal (S_1) and semi-diurnal (S_2) atmospheric tides (Chapman and Lindzen, 1970; Dai and Wang, 1999; Kowalczk, 2009; his Fig. 4.22), illustrating an air pressure-water pressure connectivity within the epikarst. This behavior was first described by Genty and Deflandre (1998) as a "wiggles" flow regime, where daily increases (decreases) in cave air barometric pressure cause reduced (enhanced) volumetric drip flow rates, and vice versa. HRC above-cave and inside-cave barometric variations are synchronous with the semi-diurnal drip cycles (Fig. 3 – panel VII). The barometric high pressure maxima at HRC are about two hours before local solar noon and two hours before solar midnight and have an amplitude of about 1 mbar, the typical lead and amplitude for the atmospheric tidal highs in panhandle Florida (the low atmospheric pressure induced by local solar heating lags high sun by about 10 h: Dai and Wang, 1999). Rainfall events (marked by arrows in Fig. 3) can cause temporary increases in drip rate. However, the saw-tooth pattern is preserved. Note that drip rates decrease when barometric pressure increases, even for cycles in which the S_1 (diurnal) cycle dominates and the S_2 signal (semi-diurnal) is absent. This "wiggles" behavior is more pronounced in HRC during falling drip rate episodes (porous flow) than during filling or full epikarst conditions where piston flow dominates, a manifestation of connections between the volume of partially-filled air voids in the epikarst and very small pressure differentials acting on

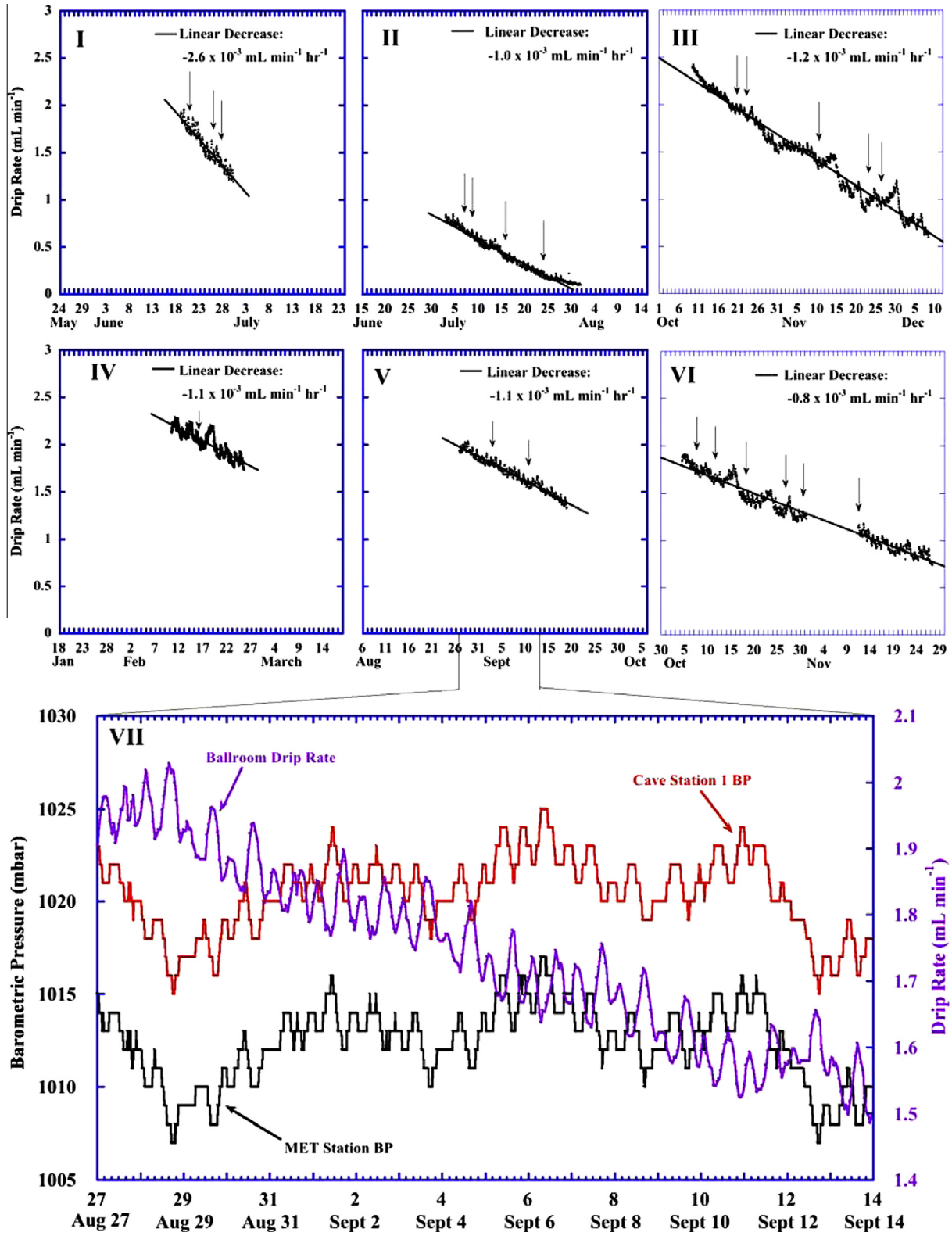

Fig. 3. Six periods of falling drip rate observed at the HRC Ballroom drip site. Each panel is an expanded view of areas labeled I through VI in Fig. 2. Linear drip loss rates (L) are shown as solid lines and are calculated for each episode as $L = (R_t - R_o)/\Delta t$ where R_o is the initial drip rate, R_t is the drip rate at time (t), and Δt is the time duration of the fall. Rainfall events are marked with downward vertical arrows. Major tick marks on time scales in panel VII are at midnight, minor tick marks are at four-hour intervals. The MET station and Cave Station 1 barometric pressures are offset by an arbitrary 8 mbars to allow visual comparison of each time series.

the air–water interfaces (air bubble compression and expansion) in the wetted capillary zone.

4.2. Rainfall and evapotranspiration controls on dripwater chemistry

Sodium (Na) and chloride (Cl) behave quasi-conservatively in forest ecosystems, especially in coastal regions with high sea salt deposition that overwhelms natural processes in the soil zone (Stallard and Edmond, 1983). Chloride in rainwater at HRC is sourced solely from sea salts in the aerosols from nearby Gulf of Mexico surface seawater. There are no evaporite deposits, nor other salt sources near HRC such as fertilized fields, septic tanks, or overlying railways or roadways (in contrast see Riechelmann et al., 2011 and Münsterer et al., 2012). HRC does not experience freeze–thaw episodes that could influence aqueous salt concentrations by 'salting out' during a freeze or diluting during a thaw cycle. Therefore we use dripwater Cl concentrations as a quasi-conservative tracer of evapotranspiration in the epikarst directly above each drip site. Cave drip and groundwaters are four to seventeen times more concentrated in Cl and three to eleven times more concentrated in Na than rainwater collected in Quincy, Florida (Table 1), consistent with our estimates of between 70% and 93% evapotranspiration (Table EA.1).

Sulfate is known to be biologically active in most forest ecosystems (Likens et al., 1970, 1996) but appears to behave conservatively at HRC. Rainfall SO_4/Cl ratios are an order of magnitude higher than sea salt and are not constant (Table 1) because local atmospheric sulfur is dominated by non-seasalt sulfate (NSS). NSS in this region likely has at least two sources; (1) oxidized dimethylsulfide (DMS), which is a marine biogenic precursor of atmospheric NSS–SO_4 particles, especially in areas of high primary productivity such as coastal Florida (Barnard et al., 1982; Andreae, 1990; Parungo et al., 1990); and (2) coal-fired power plants in the Florida panhandle region (Brezonik et al., 1980; Adams and Farwell, 1981). Cave drip and groundwaters are three to eighteen times more concentrated in SO_4 than rainwater collected in Quincy, Florida (Table 1).

Each dripwater collection site exhibits a unique clustering and range of chloride, sodium, and sulfate concentrations (Fig. 4). We take the best-fit lines through all cave and rainfall data ($[SO_4]/[Cl] = 0.42$ mol/mol and $[Na]/[Cl] = 0.86$ mol/mol) as the initial conservative rainwater and marine aerosol input ratios. All cave drip sulfate and chloride concentrations plot near the volume weighted value of rainfall $[SO_4]/[Cl] = 0.45$ mol/mol (Fig. 4a). And with the exception of Duece, all cave drips and Quincy rainwater sodium and chloride concentrations plot on the seawater [Na]/[Cl] line (Fig. 4b).

There is a weak relationship between the drip path length (DPL) and enrichments in dripwater Cl and SO_4 (Fig. EA.4a). As DPL increases, Cl and SO_4 increase along the $[SO_4]/[Cl] = 0.42$ line (Fig. EA.4c), presumably due to integrated cumulative evapotranspiration along the water flow pathway. For example, at a DPL of only 1 m, Signature Room Cl (57 μmol L^{-1}) and SO_4

Table 1
Averages and ranges for chloride (Cl^-), sodium (Na^+), and sulfate (SO_4^{2-}) concentrations in rainwater, HRC dripwaters, and HRC groundwater. See full data set in Table EC.3.

Sample location	# Samples n	Avg $[Cl^-]$ mmol L^{-1}	Range mmol L^{-1}	1σ (range) mmol L^{-1}	Avg $[Na^+]$ mmol L^{-1}	Range mmol L^{-1}	1σ (Range) mmol L^{-1}	Avg $[SO_4^{2-}]$ mmol L^{-1}	Range mmol L^{-1}	1σ (Range) mmol L^{-1}	$[SO_4]/[Cl]$ mol mol^{-1}	$[Na]/[Cl]$ mol mol^{-1}
Seawater (35 psu)		559			481			28.9			0.052	0.86
Quincy Rainfall[a]	85	0.014	0.172–0.002	0.022	0.013	0.065–0.0013	0.026	0.006	0.033–0.002	0.006	0.45	0.89
Pensacola Rainfall[b]	53	0.030	0.169–0.003	0.034	0.031	0.148–0.0009	0.032	0.011	0.025–0.003	0.006	0.37	1.03
Ballroom	37	0.112	0.129–0.101	0.007	0.095	0.158–0.088	0.011	0.063	0.070–0.057	0.003	0.56	0.84
Duece	7	0.248	0.270–0.225	0.032	0.120	0.127–0.115	0.005	0.109	0.110–0.108	0.002	0.44	0.48
Richard	1	0.058			0.036			0.021			0.35	0.62
Signature Room	3	0.057	0.066–0.048	0.009	0.062	0.065–0.060	0.003	0.020	0.024–0.015	0.005	0.36	1.09
Smith and Jones Room A	20	0.079	0.106–0.065	0.010	0.062	0.066–0.045	0.001	0.052	0.056–0.047	0.003	0.66	0.79
Smith and Jones Room B	1	0.068			0.040			0.052			0.76	0.58
Sump (Groundwater in cave)	33	0.144	0.160–0.126	0.009	0.137	0.152–0.61	0.016	0.045	0.068–0.037	0.007	0.32	0.95

[a] Quincy rainwater chemistry data provided by the National Atmospheric Deposition Program (NADP). Average values and Na/Cl and SO_4/Cl ratios are value weighted means (VWM).

[b] Pensacola rainwater chemistry data provided by William Landing, Florida State University. Average values and Na/Cl and SO_4/Cl ratios are volume weighted means.

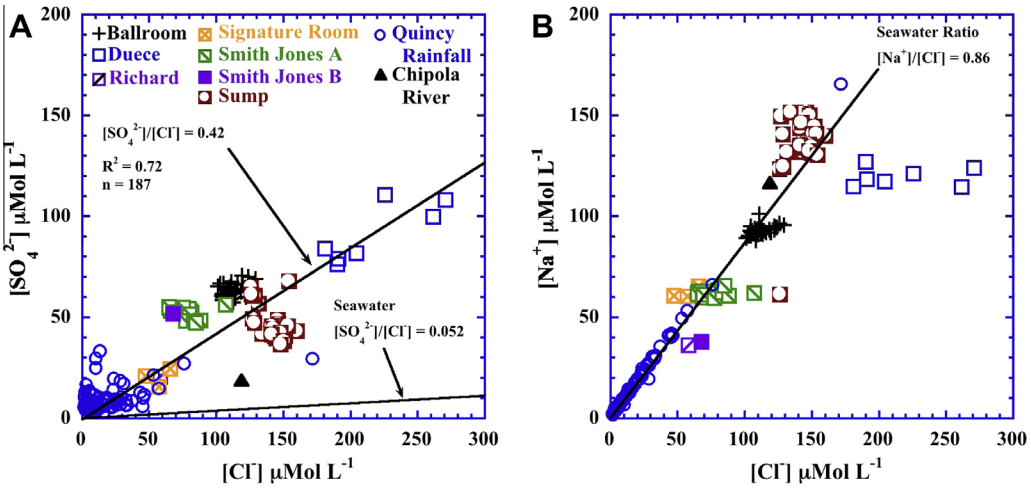

Fig. 4. (Panel A) $[SO_4^{2-}]$ vs. $[Cl^-]$ in HRC dripwaters, groundwater, Quincy rainwater, and Chipola River water. The $SO_4/Cl = 0.42$ (mol mol^{-1}) line includes all cave drips, groundwater, and rainwater. Rainwater SO_4/Cl ratios are not constant (see Table EC.3). But the rainfall volume weighted mean value ($SO_4/Cl = 0.45$; Table 1) is within error of the line. (Panel B) $[Na^+]$ vs. $[Cl^-]$ in HRC dripwaters, groundwater, Quincy rainwater, and Chipola River water. Analytical uncertainties (± 0.95 µmol L^{-1} for $[Cl^-]$; ± 0.25 µmol L^{-1} for $[SO_4^{2-}]$; ± 0.05 µmol L^{-1} for $[Na^+]$) are smaller than data symbols.

(20 µmol L^{-1}) are only slightly more concentrated than Cl and SO_4 in rainwater (Fig. EA.4a). At a DPL of 10 m, Ballroom Cl (112 µmol L^{-1}) and SO_4 (63 µmol L^{-1}) reflect a 2–3-fold flow-path enrichment due to evapotranspiration. Unlike SO_4 and Cl, the relationship between DPL and dripwater Na concentrations is not so clear (Fig. EA.4b). Dripwater Na concentrations at Signature Room, SJA, SJB, and Richard range from 36 to 65 µmol L^{-1} and exhibit little flow-path enrichment. However, drips at Sump and Ballroom are 3–5 times more enriched in Na than Richard. Na concentrations at Duece are significantly lower than expected from a conservative Na/Cl ratio. Except for Duece, HRC dripwaters exhibit conservative SO_4/Cl and Na/Cl ratios (Fig. EA.4c), but Na concentrations are not strongly correlated to DPL. Note that transpiration, which accounts forapproximately 80–90% of terrestrial water flux (Jasechko et al., 2013), does not enrich groundwater $\delta^{18}O$ or δD (Williams et al., 2004).

4.3. Bedrock and soil chemistry

As shown in Fig. 1 there are five geologic units at HRC. Soil Mg/Ca ranges from 16.7 to 139.8 mmol mol^{-1} and soil Sr/Ca ranges from 0.45 to 0.59 mmol mol^{-1}. Samples collected from the caprock along the ceiling of the Fissure Crack (TR11; see Fig. 1) are composed of dolomitic limestone with Mg/Ca ranging from 407 to 427 mmol mol^{-1} and Sr/Ca ranging from 0.43 to 0.46 mmol mol^{-1}. The presence of dolomite rhombs was verified by optical microscopy and by X-ray Diffraction (Fig. EA.5). Marianna and Bumpnose limestones are low-Mg calcite with Mg/Ca ranging from 1.6 to 14.6 mmol mol^{-1}, and Sr/Ca ranging from 0.23 to 1.0 mmol mol^{-1} (Tables 2 and EA.5). Ocala limestone is below the water table and was not sampled.

4.4. Dripwater cation chemistry

Aqueous calcium concentrations increased from 2008 through 2009 at all drip sites. However, magnesium and strontium concentrations remained relatively stable or increased slightly (Fig. EA.6). Although significant rainfall occurred in August 2008, the epikarst reached "full capacity" for only a few weeks (Fig. 2). It was not until the epikarst experienced positive net rainfall and sustained "full capacity" conditions for nearly two months that Ballroom drip water X/Ca ratios began to trend downward in February 2009 (Fig. EA.6). Thus we explicitly assign December 2008 as the end of the dry period and as the beginning of the following wet period.

Similar to $[Cl^-]$ and $[SO_4^{2-}]$, [Mg] and Mg/Ca ratios in dripwater correlate with drip path length: Mg/Ca ratios decrease *dramatically* with increasing Drip Path Length (DPL) (Fig. 5a) presumably as a result of dilution of dissolved high-Mg dolomitic caprock with dissolved low-Mg limestone along the vertical flow path. Dripwater Mg/Ca ratios are in fact strongly negatively correlated with DPL, more so than either Na/Cl or SO_4/Cl ratios. Converseley, dripwater Sr/Ca ratios tend to increase only slightly with increasing DPL (Fig. 5b).

4.5. Farmed calcite chemistry and trace element distribution coefficients

Farmed calcite Mg/Ca ranges from 1.8 to 10.5 mmol mol^{-1}, decreasing dramatically with increasing DPL. Farmed calcite Sr/Ca ranges from 0.46 to 0.90 mmol mol^{-1} and decreases slightly with increasing DPL (Table 3). All calcite X/Ca ratios are shown in Table EC.4. Cave calcite Mg and Sr distribution coefficients ($D_{Mg} = 0.031 \pm 0.008$, $D_{Sr} = 0.092 \pm 0.018$) (1σ) are in good agreement with previous cave and laboratory studies,

Table 2
Average cation concentrations and X/Ca ratios in rainwater, HRC dripwater and groundwater, and X/Ca ratios in HRC bulk limestone and dolomite with 1σ (range) at each sampling location. Seawater is shown for comparison.

Location	# Samples	Li	Na	Mg	K	Ca	Mn	Sr[a]	Si
	n	μmol L^{-1}	μmol L^{-1}	μmol L^{-1}	μmol L^{-1}	μmol L^{-1}	μmol L^{-1}	μmol L^{-1}	μmol L^{-1}
Seawater (35 psu)	–	24.5	481×10^3	54.1×10^3	10.5×10^3	10.5×10^3	0.074	92.8	103
Rainfall Pensacola[a]	53	0.009	35	3.6	3.4	4.4	0.027	0.0070	4.7
Rainfall Quincy[b]	85	0.006	17	2.2	1.3	2.8	0.018	0.0043	3.1
Ballroom	37	0.033	95	86	1.1	937	5.6×10^{-3}	0.96	37
Duece	7	0.010	120	97	2.3	1,416	7.8×10^{-3}	1.17	47
Lucky	1	0.040	43	236	7.1	1,166	11.4×10^{-3}	0.60	126
Richard	1	0.071	36	194	8.8	1,691	3.1×10^{-3}	0.72	121
Signature Room	3	0.070	62	799	2.1	1,164	2.8×10^{-3}	0.64	143
Smith and Jones Site A	20	0.092	62	412	1.8	1,046	2.3×10^{-3}	0.71	113
Smith and Jones Site A1	1	0.073	44	251	5.6	1,583	6.8×10^{-3}	0.79	123
Smith and Jones Site A2	1	0.064	42	298	7.4	1,330	4.8×10^{-3}	0.66	148
Smith and Jones Site B	3	0.045	40	242	8.6	1,087	15.1×10^{-3}	0.84	172
Sump (Groundwater)	33	0.041	139	241	12.8	1,272	8.9×10^{-3}	1.01	189
		Li/Ca	Na/Ca	Mg/Ca	K/Ca	Mn/Ca	Sr/Ca	Si/Ca	(Sr/Ca)/(Mg/Ca) Ratio
		mmol mol^{-1}	mmol mol^{-1}	mmol mol^{-1}	mmol mol^{-1}	mmol mol^{-1}	mmol mol^{-1}	mmol mol^{-1}	
Seawater (35 psu)	–	2.3	45810	5152	1000	7×10^{-3}	8.84	9.8	0.00172
Rainfall Pensacola[a]	53	2.1	8139	772	906	6.1	1.59	1068	0.00206
Rainfall Quincy[b]	85	2.2	7515	919	711	6.4	1.53	1108	0.00193
Limestone (mmol mol^{-1})	75	0.020	0.346	7.8	0.73	0.61	0.46	25.2	0.0850
Dolomite (mmol mol^{-1})	2	–	–	417.2	–	0.69	0.44	120.5	0.0010
Soil (mmol mol^{-1})	9	0.028	0.587	65.6	2.88	8.60	0.53	184.0	0.0081
Ballroom	37	0.038	109	96	1.2	6.7×10^{-3}	1.07	44	0.0112
Duece	7	0.008	89	72	1.9	6.6×10^{-3}	0.87	35	0.0121
Lucky	1	0.034	37	202	6.0	9.7×10^{-3}	0.52	108	0.0026
Richard	1	0.042	22	115	5.2	1.9×10^{-3}	0.43	72	0.0037
Signature Room	3	0.063	56	721	1.9	2.4×10^{-3}	0.57	129	0.0008
Smith and Jones Site A	20	0.091	61	408	1.8	2.2×10^{-3}	0.70	110	0.0017
Smith and Jones Site A1	1	0.046	28	159	3.6	4.3×10^{-3}	0.50	77	0.0032
Smith and Jones Site A2	1	0.048	32	224	5.6	3.6×10^{-3}	0.49	111	0.0022
Smith and Jones Site B	3	0.042	36	223	7.90	13.9×10^{-3}	0.77	158	0.0035
Sump (Groundwater)	33	0.032	112	194	10.2	7×10^{-3}	0.81	152	0.0042

[a] Pensacola rainwater data from William Landing, Florida State University.
[b] Quincy rainwater data from NADP. Quincy [Sr] values were scaled from Pensacola rainfall, calculated as $[Sr]_Q = ([Mg]_Q/[Mg]_P) \times [Sr]_P$.

and appear uniform inside HRC despite wide variations in Mg and Sr solution chemistries (Table 4). We observe no relationship between temperature and D_{Mg}. Weak relationships are observed between temperature and D_{Li}, D_K, and D_{Sr} (Table EA.4), but the lack of correlation between D_{Mg} and temperature is likely due to the small range in temperature at interior drip sites in HRC (Tremaine et al., 2011). Growth rate dependencies were not observed for any of the measured elements, including Sr (Table EA.4). The lack of correlation between D_{Sr} and growth rate is likely due to our poorly constrained slow growth rates. HRC calcite precipitates slowly compared to other caves such as those in the Edwards Plateau (Banner et al., 2007).

Distribution coefficients for Na ($D_{Na} = 0.0058 \pm 0.004$) are also uniform throughout the cave and agree with literature values. However, lithium ($D_{Li} = 0.044 \pm 0.046$) and potassium ($D_K = 0.061 \pm 0.054$) partitioning into HRC calcite are both highly variable and an order of magnitude larger than laboratory results reported by Okumura and Kitano (1986). One possible reason is because our unfiltered samples may contain sporadic contamination from cation-bearing clays in dripwaters and farmed calcite. Silicon partitioning was calculated ($D_{Si} = 0.018 \pm 0.013$) but to our knowledge has not been previously reported in the context of cave-based paleohydrologic investigations. All elements discussed here have distribution coefficients much less than unity and are thus strongly discriminated against in speleothem calcite.

5. DRIPWATER AND CALCITE CHEMISTRY – DISCUSSION

5.1. Dripwater cation chemistry

Dripwater chemistry is controlled primarily by dissolution of host carbonate rock minerals (aragonite, calcite, or dolomite). Several interchangeable terms are used in the literature to describe cation extraction from bedrock into dripwater. We use the terms 'differential dissolution' and 'preferential calcite dissolution' to mean that calcite limestone dissolves preferentially while leaving dolomite behind because the kinetics of calcite dissolution are several orders of magnitude more rapid than dolomite dissolution. We consider the terms 'incongruent (calcite or dolomite) dissolution' and 'selective leaching' to denote a preferential extraction of Mg and/or Sr from a homogeneous bedrock phase. Selective leaching occurs on fresh surfaces, but this short-lived extraction happens within the first few lattice sites of freshly crushed or cracked carbonate (Busenberg and Plummer, 1982; Fairchild et al., 1999; McGillen and Fairchild, 2005). Selective leaching of calcite does not occur in nature in older limestone beds (Palmer and Edmond, 1992). We find no evidence of incongruent dissolution at HRC, and there is no aragonite remaining in the host rocks.

Fairchild et al. (2000) considered that "*variations in the proportion of dolomite and calcite weathering due to varying residence time should result in antipathetic trends on the Mg/Ca-Sr/Ca plot*" (see their Fig. 8). Karmann et al. (2007) later noted "*variation in bedrock composition at the beginning of flow routes is possibly the cause of spatial differences in mean values of Mg and Sr between dripwaters*". Thus cave dripwater chemistry is affected by at least three factors: (1) dissolution of host bedrock and soil minerals; (2) mixing of these source solutions; and (3) pre-drip $CO_{2(aq)}$ degasing from percolating water and resulting PCP upstream of the drip during dry periods of negative net rainfall (Fairchild et al., 2000; Karmann et al., 2007; Sherwin and Baldini, 2011; Wong et al., 2011; Oster et al., 2012).

These processes can be separated by normalizing elements to calcium and by depicting their influences graphically. This approach inherently assumes that karstlimestones and dolomites dissolve congruently during weathering, and that the bedrock left behind after partial dissolution has the same bulk composition as the limestone bedrock that has been dissolved into epikarst percolation waters (as defined by Busenberg and Plummer, 1982; Morse, 2003). We do *not* assume that host dolomite dissolves at the same rate as host limestone. This approach also allows graphical isolation of 'incongruent dissolution' or 'selective leaching'.

5.1.1. A model of dripwater mixing and PCP evolution

Mixing between bedrock fluid reservoirs controls dripwater Sr/Ca and Mg/Ca ratios inside karstic caves (Fairchild et al., 2000; Tooth and Fairchild, 2003; McMillan et al., 2005). At HRC the reservoirs include dissolved limestone and dissolved dolomite. The large difference in Mg/Ca between the dolomitic capstone and the underlying low-magnesium limestone is important. Waters traveling through the dolomitic caprock carry the dolomite signature (high Mg/Ca ratios), while waters that do not travel through the dolomite carry only the limestone signature (low Mg/Ca ratios). Mixing of the two endmembers sets the initial dripwater composition.

To illustrate the concept of mixing, we depict the mixing 'domain' as the first quadrant of a clock – an XY plot of Sr/Ca vs. Mg/Ca between "Noon" and "3 pm" (shaded area in Fig. 6a). The Y-axis (clock hand at "Noon") represents pure dissolved limestone ($Sr/Mg = 0.085$ mol mol^{-1}) and the X-axis (clock hand at 3 pm) represents pure dissolved HRC dolomite ($Sr/Mg = 0.001$ mol mol^{-1}). Mixing between the two creates drip compositions that plot along a mixing arc between source-rock endmembers (see also Fairchild et al., 2000; their Fig. 8). On this clock analogue, mix-

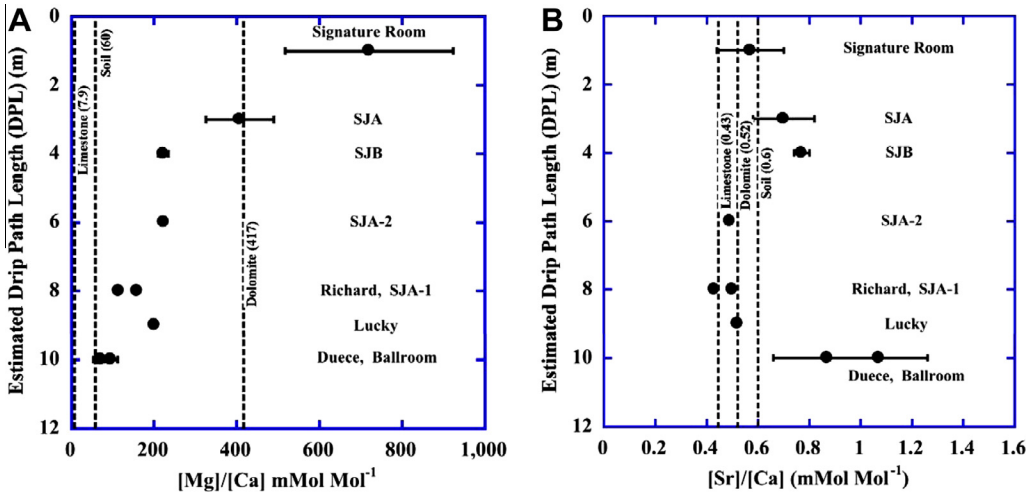

Fig. 5. (Panel A) HRC dripwater Mg/Ca ratios, plus limestone, dolomite, soil and rainfall Mg/Ca ratios (vertical dotted lines) versus estimated drip path length (DPL). (Panel B) HRC dripwater, groundwater, limestone, dolomite, and rainfall Sr/Ca ratios versus estimated DPL. Error bars are 1σ ($n = 5$) range.

Table 3
Average Mg/Ca and Sr/Ca ratios in HRC farmed calcite with DPL. Averages were calculated by summing all available data at each site and dividing by the number of data points.

Location	DPL m	Mg/Ca mmol mol^{-1}	1σ	Sr/Ca mmol mol^{-1}	1σ
Ballroom	10	1.8	0.60	0.068	0.0010
Duece	10	1.5	0.14	0.046	0.0053
Lucky	9	7.8	0.15	0.054	0.0082
Richard	8	5.1	0.67	0.050	0.0045
SJA-1	8	6.0	0.32	0.052	0.0033
SJA-2	6	9.6	0.67	0.050	0.0053
SJB-1	4	8.1	0.59	0.082	0.0093
SJB-2	4	8.9	0.09	0.074	0.0044
SJB-3	4	7.6	0.19	0.090	0.0056
SJB-5	4	8.4	0.33	0.072	0.0057
SJB-6	4	10.5	0.15	0.074	0.0051

ing between source-rock reservoirs is depicted as radials of the hour hand (Fig. 6a – dotted lines). The purple hour hand at "2 pm" points to a starting dripwater composition that is 2/3 dolomite-derived Sr and Mg and 1/3 limestone-derived Sr and Mg. Mixing fractions above each drip site are presumed constant under stable hydrologic conditions. Changes in hydrology such as altered dripwater flow paths or enhanced dissolution of one endmember over another (preferential dissolution) can shift the starting composition along the mixing arc toward the dominant endmember. In reality this mixing domain is not strictly a circular arc and does not extend to the origin, but is bounded by the natural range in bedrock Sr/Ca and Mg/Ca ratios (data presented in Table EA.3).

After mixing between limestone and dolomite endmember solutions, dripwaters then evolve via Prior Calcite Precipitation (PCP) from this 'starting' composition toward higher X/Ca ratios along vectors of almost constant Sr/Mg slope (Fig. 6a – dashed lines). These model vectors predict the stepwise evolution of dripwaters as calcite PCP progressively excludes magnesium and strontium from the solid phase and enriches them in the residual solution (after Fairchild and Baker, 2012):

$$Sr_i = Sr_o - (Ca_i - Ca_o)(D_{Sr}) \quad (1)$$

$$Mg_i = Mg_o - (Ca_i - Ca_o)(D_{Mg}) \quad (2)$$

and

$$\Delta Ca = Ca_i - Ca_o \quad (3)$$

where Sr_o, Mg_o, and Ca_o are the initial compositions at each step, Sr_i, Mg_i, and Ca_i are the 'new' incremental dripwater compositions, and ΔCa is the arbitrary small step increment of calcium precipitated from solution as PCP-calcite ($CaCO_3$). On a Sr/Ca vs. Mg/Ca plot, PCP vectors (see Table EC.6 for calculations) can be described by:

$$\frac{\Delta Sr}{\Delta Ca} = \frac{Sr_o - \Delta Ca(D_{Sr})}{\Delta Ca} \quad (4)$$

and

$$\frac{\Delta Mg}{\Delta Ca} = \frac{Mg_o - \Delta Ca(D_{Mg})}{\Delta Ca} \quad (5)$$

Rearrangement of Eqs. (4) and (5) gives the PCP slope:

$$\frac{\Delta Sr}{\Delta Mg} = \frac{Sr_o - \Delta Ca(D_{Sr})}{Mg_o - \Delta Ca(D_{Mg})} \quad (6)$$

From a given starting composition (Sr_o and Mg_o), dripwater chemistry evolves along these PCP vectors as $CaCO_3$ (ΔCa^{2+}) is precipitated and Mg and Sr are discriminated against and thus enriched in the residual solution. Example post-PCP drip compositions are represented by solidred squares on Fig. 6a. According to Eq. (6) the slope of each PCP vector is constant, and is set by: (1) the ratio of distribution coefficients (D_{Sr}/D_{Mg}); and (2) the initial 'mixed' source composition Sr_o/Mg_o ratio. As we will show below, the location along each vector, or the extent of PCP production, is controlled by the balance between rainfall and evapotranspiration (P−ET). Note that PCP vectors are not radials on Fig. 6a, but are slanted to the right (rotated clockwise) since the ratio of distribution coefficients is greater than one (D_{Sr}/D_{Mg} ~3). See Appendix EB.3 for discussion of this graphical characteristic and Table EC.6 for example calculations.

During very wet conditions (P−ET > 1), CO_2 degasing from soil and karst waters into air-filled voids within the epikarst is suppressed. Hydraulic loading promotes higher drip rates, which in turn reduces the amount of time available for CO_2 degasing at each soda straw or stalactite. Both of these factors reduce PCP production, driving drip composition inward along PCP vectors back toward dissolved bedrock. If the epikarst were at 'full-pool' and draining so rapidly as to entirely halt PCP, dripwater Mg/Ca and Sr/Ca compositions would simply remain at the mixed starting composition of dissolved bedrock and would not evolve out the PCP vector.

During dry conditions (P−ET < 1), evapotranspiration removes water from the overlying soil and bedrock, lowering the top of the wetted saturation zone and creating air voids that promote dripwaters to degas CO_2. As bedrock fluid reservoirs slowly empty, the void space becomes more prominent. Reduced hydraulic loading decreases drip rates (see Figs. 2 and 3), which further increases the time available for dripwaters to degas CO_2 at soda straw and stalactite tips. Both of these conditions promote PCP. Therefore the distal outer ends of each PCP vector represent very dry conditions with a larger extent of PCP.

It is important to note that after bedrock dissolution and mixing have occurred, subsequent rainwater or evapotranspiration driven changes in PCP production will drive drip chemistry outward (dry) or inward (wet) along the PCP vector but will not significantly alter Sr/Mg ratios. Evaporation and dilution do not affect this treatment of PCP because (Mg/Cl)/(Ca/Cl) = Mg/Ca and (Sr/Cl)/(Ca/Cl) = Sr/Ca (i.e., enrichment by evapotranspiration or dilution by adding rainwater does not alter Sr/Mg). Said another way, variable mixing between bedrock reservoirs can alter dripwater Sr/Mg ratios, but PCP alters Sr/Mg ratios only according to the ratio of the D_Xs. Inherent in this concept is that once limestone has dissolved and re-precipitated as the new diagenetic calcite phase (PCP), this diage-

Table 4
Averaged distribution coefficients (D_X-in bold) of modern calcite farmed *in situ* at drip sites in HRC and values from the literature for inorganic calcites. HRC averages were calculated by summing all available data at each site and dividing by the number of data points (see Table EA.2). Coefficients are calculated as $D_X = \frac{(X/Ca)_{CaCO_3}}{(X/Ca)_{Aq}}$ and are reported in units of [mmol mol^{-1}/mmol mol^{-1}]. See Table EC.1 for all data used to calculate D_X.

	D_{Mg}	Max Min	D_{Sr}	Max Min	D_{Na}	Max Min	D_{Li}	Max Min	D_K	Max Min	D_{Mn}	Max Min	D_{Si}	Max Min
Cave studies														
This study (speleothem)	**0.031**	0.041 0.019	**0.092**	0.112 0.061	**0.0058**	0.0150 0.0030	**0.044**	0.13 0.01	**0.061**	0.15 0.007	**4.9**	9.5 0.7	**0.018**	0.041 0.003
Holland et al. (1964a)			**0.140**	0.160 0.120										
Gascoyne (1983)	**0.035**	0.057 0.013	**0.130**	0.298 0.088										
Huang and Fairchild (2001)	**0.031**	0.038 0.014	**0.075**	0.111 0.057										
Huang et al. (2001)[a]	**0.014**	0.016 0.012	**0.155**	0.160 0.150										
Stern et al. (2005)[b]	**0.023**		**0.120**											
Karmann et al. (2007)[b]	**0.023**		**0.059**											
Fairchild et al. (2010)	**0.0177**	0.020 0.015	**0.110**	0.130 0.079										
Laboratory studies														
Holland et al. (1964b)			**0.076**	0.102 0.056										
Kitano et al. (1971)[c]			**0.081**	0.400 0.080										
Katz et al. (1972), Katz (1973)[d]	**0.097**	0.124 0.057	**0.070**	0.170 0.050										
Lorens (1978, 1981)			**0.054**	0.126 0.031							**14.6**	33 5		
Mucci and Morse (1983)	**0.019**	0.032 0.010	**0.27**	0.400 0.150										
Pingitore and Eastman (1984, 1986)			**0.08**	0.193 0.030										
Okumura and Kitano (1986)					**0.002**	0.006 0.001	**0.004**	0.009 0.003	**0.00005**	0.0020 0.0005				
Zhong and Mucci (1995)					**0.0006**	0.0040 0.0002								
Tesoriero and Pankow (1996)			**0.021**	0.140 0.020										
Gabitov and Watson (2006)			**0.12**	0.350 0.120										

[a] D_X values were reported for stalagmites (Max number) and stalactites (Min number).
[b] Only average D_X values were reported.
[c] Both calcite and aragonite were precipitated in these studies, however only calcite numbers are reproduced here.
[d] Pure aragonite was precipitated from solution, then recrystalized into calcite at various experimental durations.

netic calcite phase is thermodynamically more stable than the surrounding limestone (Berner, 1981). Thus we make the explicit assumption that PCP-calcite does not dissolve in the presence of limestone and that dripwater starting composition represents only mixing between dissolved bedrock phases. If PCP-calcite *were* to dissolve it would be quite apparent on a Sr/Ca vs. Mg/Ca plot. A discussion of how PCP-calcite dissolution can be chemically identified in dripwater is presented in EB.3.

5.1.2. Measured drip chemistry

Aqueous cation chemistry, like anion chemistry, is distinct at HRC each drip site (Fairchild et al., 2000, 2006; Verheyden et al., 2000; Huang et al., 2001; Musgrove and Banner, 2004; Spötl et al., 2005; Baldini et al., 2006; Guilfoyle, 2006; McDonald et al., 2007; Wong et al., 2011; Riechelmann et al., 2011). Drip sites with long DPL (e.g., Duece) have higher Sr/Mg slopes than those with shorter DPL (e.g., Smith and Jones A or Signature Room), suggesting lower proportions of dissolved dolomite (and higher dissolved limestone) with increasing vertical distance below the dolomitic caprock (Fig. 6b). PCP vectors were calculated from Eqs. (4) and (5) at several source rock mixing ratios (i.e., at 6%, 20%, 37%, and 80% dolomite) and are represented by dashed lines on Fig. 6b (see Table EC.6 for calculations). PCP vectors were derived from common starting conditions of

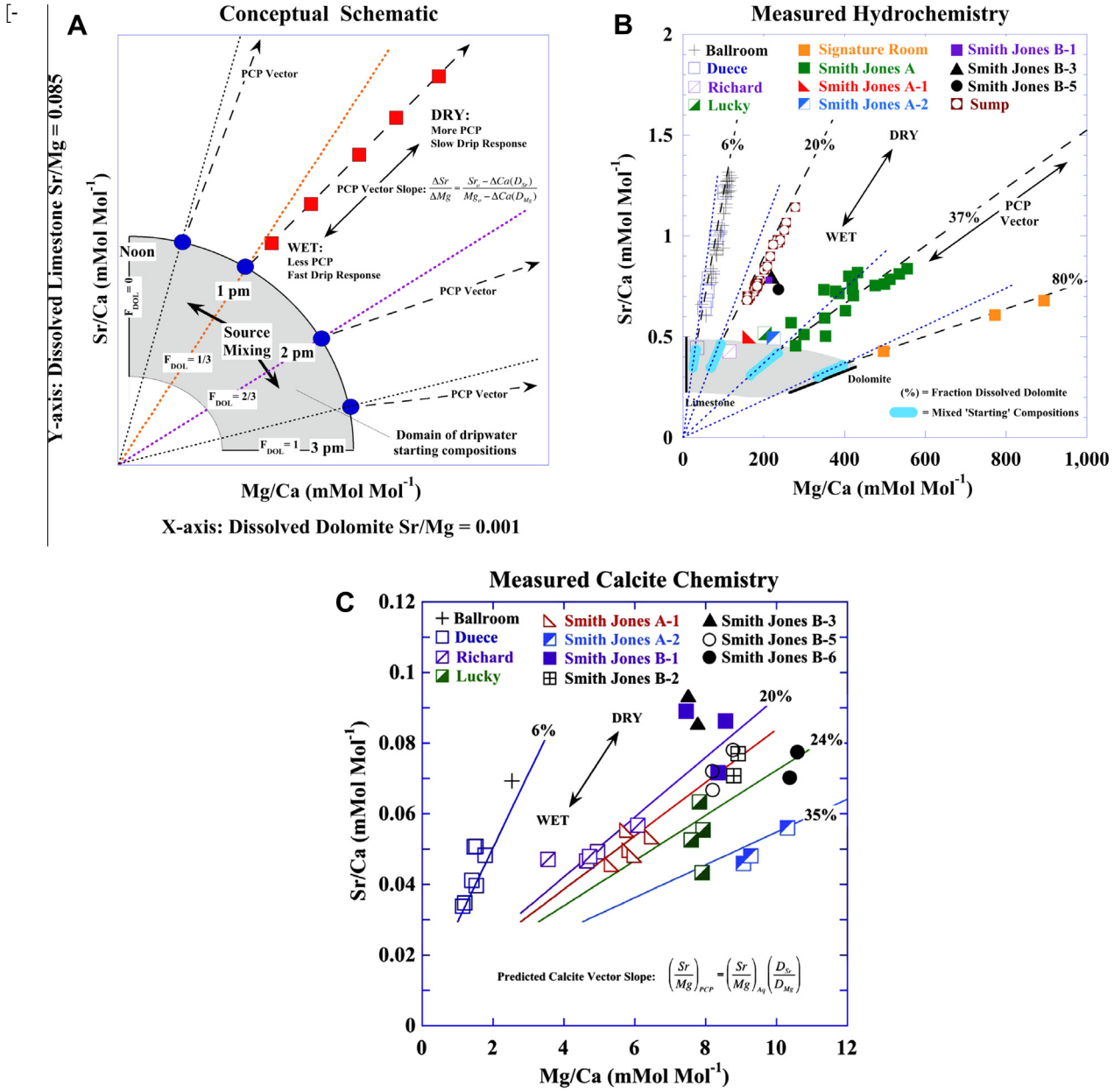

Fig. 6. (Panel A) Conceptual schematic of the predicted evolution of cave dripwaters as a function of only two geochemical processes: (1) mixing between dissolved bedrock endmembers (limestone and dolomite); and (2) Prior Calcite Precipitation (PCP). We depict the dissolved bedrock "mixing regime" as radials on a Sr/Ca vs. Mg/Ca plot, illustrated schematically as a clock quadrant between 12 pm and 3 pm (gray shaded area). Mixing between dilute rainwater (the origin, $x = 0$, $y = 0$) and these two dissolved geochemical endmembers results in dripwater compositions that lie within a continuous mixing zone (depicted as the gray arc). Fractional mixing sets the "initial" dripwater composition (solid blue circles are examples). Drip chemistry then evolves away from the dissolved bedrock source mixture toward higher Sr/Ca and Mg/Ca ratios. Note that all PCP vectors are slanted to the right (rotated clockwise) of each mixing radial (dashed lines vs. dotted lines). Wet period drip chemistry trends *inward* along PCP vectors. Dry period Sr/Ca and Mg/Ca trend *outward* toward the distal ends of PCP vectors. (Panel B) Measured Sr/Ca vs. Mg/Ca in HRC dripwaters and groundwater. Short solid black lines depict average measured limestone and dolomite Sr/Mg ratios (Table 2). The gray arc illustrates the domain where endmember mixing fixes the 'starting' composition of dripwaters (values from Table 2). Dotted lines labeled 6% to 80% are PCP vectors modeled from different dissolved limestone bedrock mixtures (light blue ovals). (Panel C) Sr/Ca vs. Mg/Ca ratios in HRC farmed calcite plotted with predicted calcite chemistry vectors at each site. See Electronic Annex B for a discussion of the graphical characteristics of these PCP plots.

$Ca^{2+}] = 2500$ μmol L^{-1}, a *calculated* pH = 6.88 (see pH calculation in Table EC.8), *measured* mean soil $pCO_2 = 4{,}077$ ppmv, $D_{Mg} = 0.031$, $D_{Sr} = 0.092$, and aquatic carbonate equilibrium constants at 20 °C (after Pilson, 1998) where dripwater is assumed saturated with respect to calcite ($\Omega = 1.0$). Initial Mg and Sr starting conditions are chosen from arbitrary points inside the mixing domain

Table 5
Response relationships between drip chemistry, calcite chemistry, and fluctuations in rainfall and *in situ* drip rates. Changes in drip rate, dripwater X/Ca ratios, and calcite X/Ca ratios for each site are taken as two-point differences between the beginning and end of the sample period. The symbol (Δ) denotes 'change' or 'difference'.

Table row	Location	Sample period	Δ Drip rate (mL min^{-1})	*Hydrochemical response* $\Delta(X/Ca)_{H_2O}/\Delta$(drip rate) mmol mol^{-1}/mL min^{-1}		
				Na/Ca	Mg/Ca	Sr/Ca
1	Ballroom	12/2009–2/2010	+1.80	−28	−22	−0.25
2	Duece	11/2009–2/2010	+0.44	−91	−73	−0.88
3	Smith and Jones A	9/2009–1/2010	+1.20	−29	−235	−0.33
				Speleochemical response $\Delta(X/Ca)_{CaCO_3}/\Delta$(drip rate) mmol mol^{-1}/mL min^{-1}		
				Na/Ca	Mg/Ca	Sr/Ca
4	Duece	11/2009–2/2010	+0.44	−0.57	−0.16	−0.023
			Δ Net rainfall (mm)	*Speleochemical rainfall response* $\Delta(X/Ca)_{CaCO_3}/\Delta$(net rainfall mmol mol^{-1}/mm		
				Na/Ca	Mg/Ca	Sr/Ca
5	Duece	11/2009–2/2010	+33	-7.6×10^{-3}	-21×10^{-4}	-3×10^{-4}

Δ Drip Volume calculated from a measured 0.12 mL $drip^{-1}$ (Tremaine, 2010).
Δ Net Rainfall calculated from Table EA.1 as $[(NR_{Dec\,2009} + NR_{Jan} + NR_{Feb\,2010})/3] - [(NR_{Sept} + NR_{Oct} + NR_{Nov\,2009})/3]$.

where dolomite fraction is defined by Mg/Ca and Sr/Ca ratios. These points adequately represent this system.

As a test for sensitivity of pH to starting conditions, we tested these calculations over a range of $[Ca^{2+}]$ from 1500 to 3500 μmol L^{-1} (resulting pH ~6.80 to 6.99), a range of pCO_2 from 3700 to 5700 ppmv (resulting pH ~6.83 to 6.94), and a range of temperatures from 15 to 25 °C (resulting pH ~6.85 to 6.91). This wide range of inputs has little impact on pH, suggesting that pH is well buffered in the soil–limestone system (see Table EC.8).

Drip chemistries at Ballroom and Duece range from dissolved bedrock composition to highly enriched Mg/Ca and Sr/Ca compositions, reflecting periods of both very wet and very dry rainfall conditions (Fig. 6b). Ballroom and Duece drip chemistries closely mimic the PCP vector modeled from a 6% dolomite contribution, suggesting that: (1) their bedrock-mixing ratios are the same; (2) the mixing ratios are constant; and (3) PCP is the only process affecting post-mixing chemical evolution at these sites. Furthermore their chemistry suggests that even at the deepest point in the cave (Ballroom and Duece have the longest DPLs) the dolomitic caprock contributes a measurable portion of magnesium in dripwater.

Smith and Jones A (SJA) drip chemistry plots around a 37% dolomite PCP vector. This scatter suggests that the bedrock-mixing ratio of the water supplying SJA is not constant, but oscillates along the mixing arc between about 30% and 44% dolomite (these vectors not shown). One important characteristic of the SJA drip site is that even though the mean drip rates are higher than almost all other sites (see Fig. EA.3), SJA is usually the last site to stop dripping during dry periods. This suggests that SJA underlies a larger reservoir than other drips. Bi-weekly grab-sample drip rate information at SJA is not sufficient to test if there is a correlation between drip rate and Sr/Mg ratios. But SJA dripwater Sr/Mg ratios that plot to the left of the PCP vector are coincident with the period of Ballroom drip rate *decline* between August 29th, 2009 and November 21st, 2009. As discussed in Section 4.1, this period is characterized by a shift from piston flow to porous flow at the Ballroom site. This suggests that SJA drips have more dolomite-derived magnesium during very wet periods when the bedrock fluid reservoir is filled to the stratigraphic level of the dolomitic caprock. Conversely, SJA drips contain less dolomite-derived magnesium during dry periods when reservoir fluid levels fall below the contact point with dolomitic caprock.

Signature Room (SR) dripwaters closely mimic the 80% dolomite PCP vector, suggesting a constant bedrock-mixing ratio with magnesium concentrations higher than all other drip locations. The SR is directly overlain by dolomitic limestone (DPL < 1 m), thus SR dripwater starting composition has the highest Mg/Ca ratios. The SR drips are active only after heavy rainfall events and are classified as shaft-flow drips (Fig. EA.3).Under even high-flow conditions, degasing and PCP along the 4–5 m tall flowstone drapery that transmits ceiling flow to the drip site is sufficient to significantly increase Mg/Ca ratios.

Sump chemistry closely follows a 20% dolomite PCP vector, suggesting a constant bedrock-mixing ratio that probably reflects the average post-PCP groundwater composition below the cave. Drip chemistries at Richard, SJA-1, SJA-2, and SJB plot between those of Sump and SJA. There are insufficient data at these sites to evaluate the constancy of their bedrock-mixing ratios or their sensitivities to wet vs. dry hydrologic effects on PCP.

Dry period (2008) drip waters have lower [Ca] (higher extent of PCP), while 2009–2010 drips have increasing [Ca] from dissolved bedrock and decreased extent of the

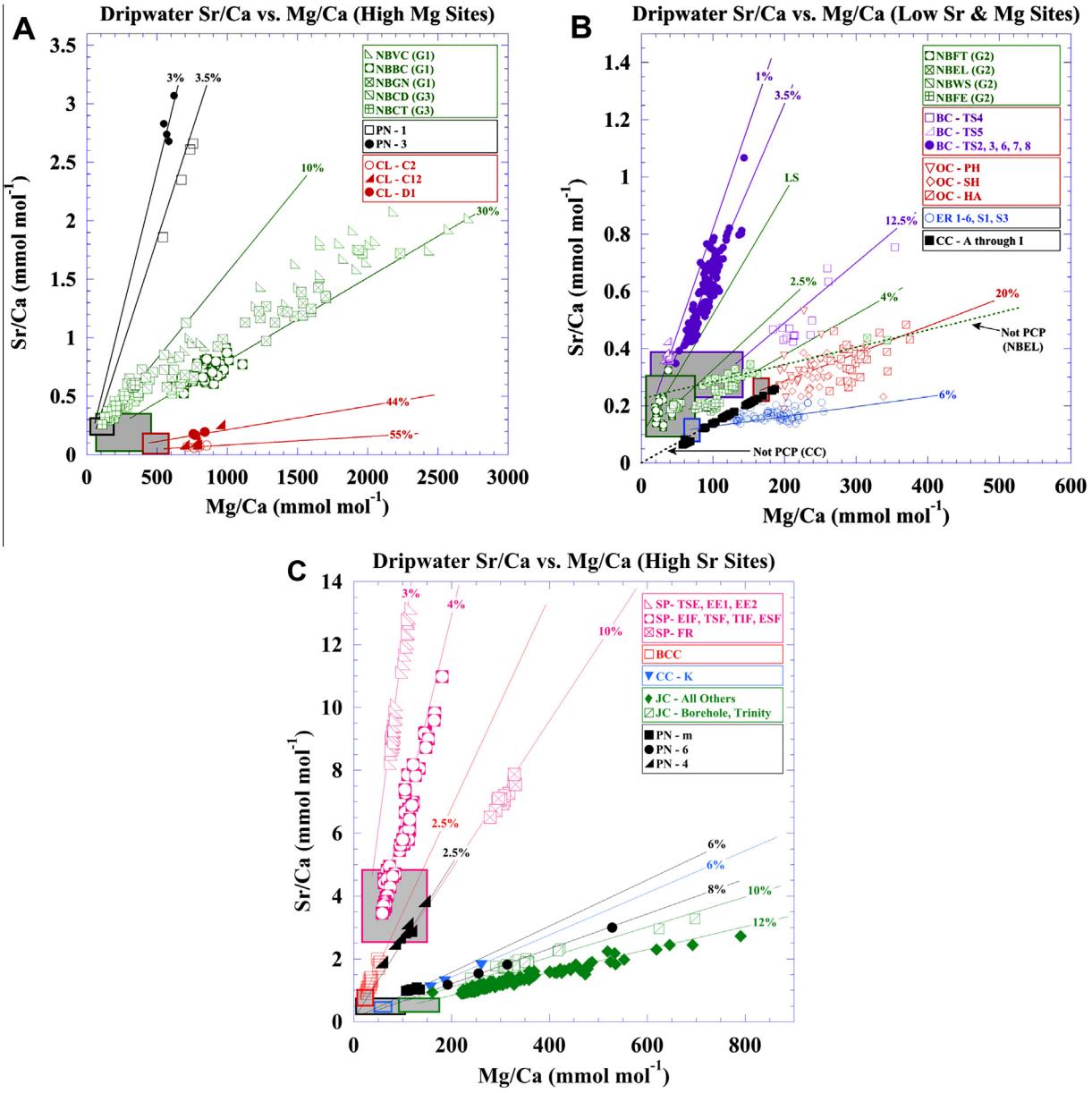

Fig. 7. Published dripwater Sr/Ca and Mg/Ca data plotted with PCP vectors for each cave end-member starting bedrock composition (see Table EA.5). (Panel A) Dripwater Sr/Ca vs. Mg/Ca ratios at published high-magnesium sites: Natural Bridge Caverns (NB) (Wong et al., 2011); Père Nöel Cave (PN) (Verheyden et al., 2008; their Fig. 13); and Clamouse Cave (CL) (Fairchild et al., 2000). PCP vectors are plotted with slightly different mixed-bedrock starting compositions based on bedrock chemistry at each cave, illustrated as grey boxes with cave specific colors (see Table EA.5). Dolomite mixing fractions for each cave are a function of mixed starting compositions and do not necessarily overlap with other caves. (Panel B) Dripwater Sr/Ca vs. Mg/Ca ratios at published low-strontium and low-magnesium sites: Crag Cave (CC) (Tooth and Fairchild, 2003); Natural Bridge Caverns (NB) (Wong et al., 2011); Bunker Cave (BC) (Riechelmann et al., 2011); Obir Cave (OC) (Spötl et al., 2005); and Grotta di Ernesto (ER) (Fairchild et al., 2000). (Panel C) Dripwater Sr/Ca vs. Mg/Ca ratios from published high-strontium sites: Santana-Pérolas Cave (SP) (Karmann et al., 2007; their Fig. 8); Black Chasm Cavern (BCC) (Oster et al., 2012); Crag Cave (CC) (Tooth and Fairchild, 2003); Jinapsan Cave (JC) (Partin et al., 2012); and Père Nöel Cave (PN) (Verheyden et al., 2008; their Fig. 13).

PCP reaction. See Fig. EA.6 for [Ca], [Mg], and [Sr] time series. Dripwater Sr/Ca and Mg/Ca ratios at each site tended to migrate along nearly constant Sr/Mg PCP vectors toward the origin of the axes (dissolved bedrock-mixing domain) during very wet periods, and away from the origin of the axes during dry periods. This is illustrated by diagonal arrows in Fig. 2b; blue down-arrows indicate *reduced* PCP during periods of increasing or very high drip rate, and red up-arrows indicate *increased* PCP during periods of falling or very low drip rates. These migrations in Mg/Ca and Sr/Ca (and other X/Ca) ratios at Ballroom, Duece, and SJA are illustrated in Figs. EA.6 and EA.7. This is a serendipitous result that allows us to unambiguously calibrate be-

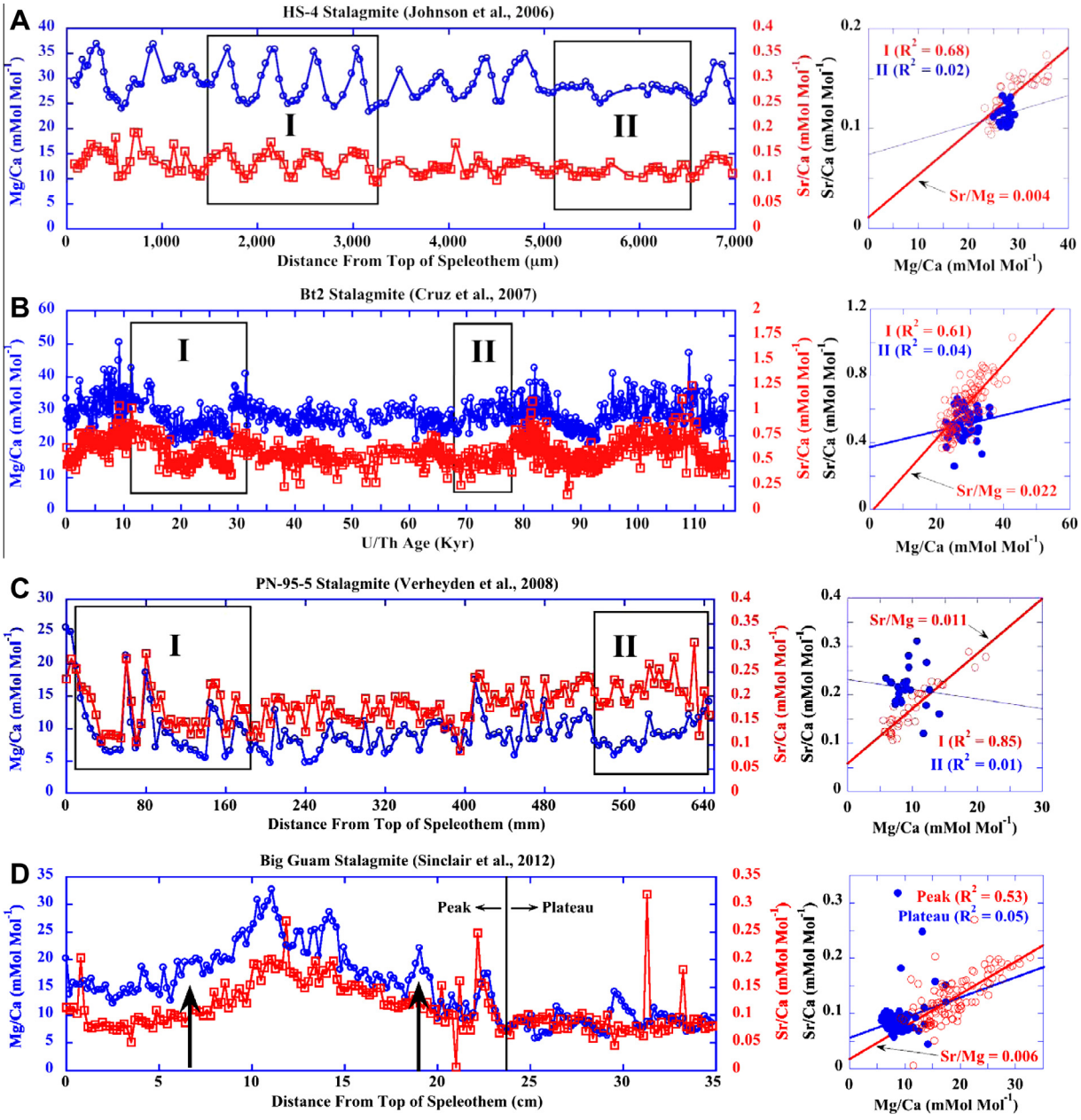

Fig. 8. Published speleothem geochemical records. The symbology is the same for panels A, B, C and D. (Panel A) Speleothem Sr/Ca (red open squares; right Y-axis) and Mg/Ca (blue open circles; left Y-axis) timeseries record from Heshang Cave (China) stalagmite HS-4 (Johnson et al., 2006; their Fig. 5) and a Sr/Ca vs. Mg/Ca (Sr vs. Mg) crossplot of data from a correlated section (box I: red open circles, from 1481 to 3296 μm) and an uncorrelated section (box II: blue closed circles, from 5051 to 6579 μm). (Panel B) Speleothem Sr/Ca and Mg/Ca timeseries record from Botuverá Cave (Brazil) stalagmite Bt2 (Cruz et al., 2007; their Fig. 3) and a crossplot of data from a correlated section (box I: from 11.1 to 33.3 Kyr) and an uncorrelated section (box II: from 67.05 to 77.78 Kyr). (Panel C) Spleothem Sr/Ca and Mg/Ca timeseries record from Perè Noël Cave (Belgium) stalagmite PN-95-5 (Verheyden et al., 2008; their Fig. 19) and a crossplot of data from a correlated section (box I: from 10 to 190 mm) and an uncorrelated section (box II: from 530 to 645 mm). (Panel D) Speleothem Sr/Ca and Mg/Ca timeseries record from Jinapsan Cave (Guam Island) stalagmite "Big Guam" (Sinclair et al., 2012; their Fig. 2) and a crossplot of data from both the correlated "Peak" (from 0 to 24 cm) and the uncorrelated "Plateau" (from 24 to 35 cm). Constant Sr/Ca vs. Mg/Ca (Sr/Mg) ratios in these records suggest that these stalagmites precipitated from drips with constant dissolved bedrock-mixing ratios. Fluctuations in Sr/Ca and Mg/Ca in correlated sections can thus be interpreted as a PCP-modulated wet versus dry records. (For interpretation of the references to color in this figure legend, the reader is referred to the web version of this article.)

tween dripwater chemistry and calcite chemistry during

both wet and dry periods.

5.2. Farmed calcite chemistry

To test whether speleothems preserve chemical fluctuations in drip chemistries, we compare modern farmed calcite (equivalent to PCP-calcite) to coeval dripwaters on a Sr/Ca vs. Mg/Ca plot (Fig. 6c). We take an approach similar to modeling PCP vectors by calculating the predicted vector of calcite chemistry evolution as a function of measured dripwater composition and distribution coefficients at each site. We estimate vertical and horizontal vectors as:

$$\left(\frac{Sr}{Ca}\right)_{PCP} = \left(\frac{Sr}{Ca}\right)_{Aq}(D_{Sr}) \quad (7)$$

and

$$\left(\frac{Mg}{Ca}\right)_{PCP} = \left(\frac{Mg}{Ca}\right)_{Aq}(D_{Mg}) \quad (8)$$

where subscript 'PCP' denotes farmed calcite, and 'Aq' denotes cations in solution. Rearrangement of these two equations gives the predicted vectors (slopes) of calcite PCP evolution:

$$\left(\frac{Sr}{Mg}\right)_{PCP} = \left(\frac{Sr}{Mg}\right)_{Aq}\left(\frac{D_{Sr}}{D_{Mg}}\right) \quad (9)$$

We make two assumptions in this approach: (1) that distribution coefficients are nearly constant under the range of modern cave temperature and growth rate conditions; and (2) that calcite growth rates are slow and therefore insensitive to very short-term (1–2 week) fluctuations in dripwater chemistry associated with large rainfall events.

Farmed calcite chemistry displays chemical groupings similar to those of dripwaters (Fig. 6c), trending from dry-period higher Mg/Ca and Sr/Ca ratios to wet-period lower ratios. Duece and Ballroom calcite plots along the evolution vector predicted from Duece dripwater Sr/Mg compositions, suggesting that Duece and Ballroom calcites faithfully record changes in Mg/Ca and Sr/Ca in dripwater. Calcite at Richard, SJA-1, SJA-2, SJB-2, SJB-3, and SJB-6 also plot near predicted calcite evolution vectors suggesting that calcites at those sites successfully archive contemporaneous hydrochemical trends in their parent dripwaters.

Calcite at Smith and Jones sites B1 and B3 plot at higher Sr/Ca than the predicted 20% dolomite calcite evolution vector. Lucky calcite scatters around the 24% dolomite evolution vector (Fig. 6c). One likely reason for the scatter in data is that bedrock-mixing ratios at these three sites may not be constant, but are oscillating between geochemical endmembers as a function of *net* rainfall. Indeed only a 15 percent change in endmember contributions is needed to explain the range in Lucky calcite chemistry. We do not have sufficient dripwater data at these sites to fully develop such an argument, and more data is needed to understand site-specific changes in hydrochemistry at each drip site. In general calcite Sr/Ca and Mg/Ca ratios (Sr/Mg ratios) trend with observed dripwater chemistry as a simple function of distribution coefficients.

5.3. Calibrating hydrogeologic conditions to dripwater and calcite chemistry – An attempt at response functions

In Section 4.1 we demonstrated a direct link between increased monthly *net* rainfall [P−ET], increased drip rate, and decreased water response time. To directly test the hypothesis that changes in *net* rainfall can contribute to variations in calcite chemistry, we monitored rainfall amount, evapotranspiration, drip rates, dripwater chemistry, and calcite chemistry at sufficient resolution to evaluate geochemical variability in modern calcite at the Ballroom, Duece, and Smith and Jones A sites. Duece was the only site where calcite growth was fast enough to monitor subseasonal variations in speleochemistry. Therefore we use the limited data available at Duece to attempt a four month two-point snapshot calibration of modern calcite chemical variation versus net rainfall, an interpretation that is frequent in the literature (see review by Fairchild and Treble, 2009).

Changes in dripwater X/Ca ratios with respect to changes in drip rates [$\Delta(X/Ca)_{Aq}/\Delta$(Drip Rate)], which we call the *hydrochemical response*, exhibit negative relationships at all sites: cation $(X/Ca)_{Aq}$ ratios *decrease* as drip rates *increase* (Table 5, Rows 1, 2, and 3). This response is expected if increased hydrologic saturation, reduced void space, and increased drip rates promote a reduction in the extent of PCP. It is important to note that although changes in $(Sr/Ca)_{Aq}$ ratios are similar at all sites, the SJA *response* in $(Mg/Ca)_{Aq}$ is ten times stronger than at the Ballroom drip site. For a given increase or decrease in PCP production in a cave, drip sites with higher dolomite mixing ratios have proportionally higher responses in Mg/Ca ratios while exhibiting the same range in Sr/Ca. It is equally important to recognizethat even though Ballroom and Duece are only a few meters apart *and* are subject to the same *net* rainfall *and* share a common dissolved bedrock source *and* have similar mixing fractions, they exhibit a threefold difference in *hydrochemical response*. This illustrates the heterogeneity of drip geochemistry to drip rate response, and suggests that relationships between dripwater response and residence time are unique at each site.

The change in Duece farmed calcite X/Ca ratios with respect to the change in drip rate [$\Delta(X/Ca)_{CaCO3}/\Delta$(Drip Rate)], which we call the *speleochemical response* (Table 5, Row 4), exhibits a negative relationship: X/Ca_{CaCO3} ratios *decrease* as drip rates *increase*. Calcite chemistry at Duece also displays a negative response to changes in *net* rainfall [$\Delta(X/Ca)_{CaCO3}/\Delta$(*Net* Rainfall)], which we call the *speleochemical rainfall response*. For this calibration ΔNet Rainfall was calculated as the difference between autumn *net* rainfall (average of Sept., Oct., and Nov. 2009) and winter *net* rainfall (average of Dec., Jan., and Feb. 2010) to approximate a seasonal change. Thus the seasonal speleochemical rainfall responses in Duece calcite are: -21×10^{-4} mmol mol^{-1}/mm for Mg/Ca, -3×10^{-4} mmol mol^{-1}/mm for Sr/Ca, and -7.6 mmol mol^{-1}/mm

for Na/Ca (Table 5, Row 5). We find that hydrologically driven variations in dripwater chemistry at the Duece farming site *are preserved* in modern calcite at a level well within the limits of detection. This is an important first step in quantifying the speleochemical response to climate-induced variability in dripwater trace element ratios.

6. DRIPWATER AND CALCITE CHEMISTRY – INTERPRETATIONS

6.1. Application of bedrock-mixing and PCP to other cave systems

We have demonstrated that the likely controls on dripwater and speleothem geochemistry in HRC are bedrock-mixing and PCP, ideas championed initially by Fairchild et al. (2000) and later by Karmann et al. (2007). Hollow Ridge Cave is a shallow, horizontal, well-ventilated cave with two chemically distinct bedrock layers and significant monthly rainfall. It is a simple cave that provides clear examples of bedrock-mixing and PCP. To see if these principles can be applied more broadly, we test our interpretations from HRC with published data in other more complex cave systems where bedrock-mixing was not recognized or was not fully developed.

These caves represent a wide range of geological characteristics and are hosted in limestone with inferred dolomite and/or high-magnesium carbonate (reefal) components and in a few cases, aragonite. In most cases the complete host rock compositions are not well known. For simplicity we use the following parameters for all these caves: limestone Mg/Ca = 9.0 mmol mol^{-1}, stoichiometric dolomite Mg/Ca = 1000 mmol mo1^{-1}, $D_{Sr} = 0.092$, and $D_{Mg} = 0.031$. For each dataset, the Sr/Ca starting values used to initiate PCP vectors are taken as the lowest, average, and highest dripwater values reported in each study, presumed to reflect host bedrock (Table EA.5). Only drip sites with three or more data points in a 1-year period are considered. These published cave data are here classified according to their hydrochemical characteristics; high-magnesium dripwaters (Fig. 7a), low-magnesium and low-strontium dripwaters (Fig. 7b), and high-strontium dripwaters (Fig. 7c). The details and nuances of plotting and interpreting these PCP graphs are discussed in EB.2. A complete discussion of each cave and drip site is provided in Electronic Annex D.

Bedrock-mixing fractions are constant to within ±3% at every site except Natural Bridge sites NBFT and NBEL. Post-mixing dripwater evolution is controlled by PCP at every site except for two: (1) NBEL drip chemistry (Fig. 7b) does not follow a PCP vector, but instead exhibits a large enrichment in Mg/Ca with nearly constant Sr/Ca that may be a fortuitous result of increasing proportions of dissolved dolomite in the mixing fraction during a dry-period enhancement in PCP; and (2) Crag Cave sites A through J (Fig. 7b) plot along a mixing radial that extends through (0,0) without exhibiting a clockwise rotation away from the radial indicative of PCP. As observed at Crag Cave, PCP does not always accompany bedrock-mixing. Application of this concept to other caves demonstrates that drip chemistries in caves are most easily explained by dissolved bedrock-mixing followed by hydrochemical evolution due to PCP. Our approach of quantifying *both* dissolved bedrock-mixing *and* extent of PCP provides a simple graphical tool to diagnose hydrochemical behavior. One important observation of this analysis is that drip waters controlled by bedrock-mixing and PCP fall along nearly constant Sr/Mg slopes despite large variations in Mg/Ca and Sr/Ca ratios.

6.2. Applying modern calibrations to ancient stalagmites

Speleothem time series records of Sr/Ca and Mg/Ca have been interpreted traditionally as proxies for prevailing hydrologic conditions; wet periods with less PCP (lower Sr/Ca and Mg/Ca ratios) versus dry periods with more PCP (higher Sr/Ca and Mg/Ca ratios) (Fairchild and Baker, 2012). To test this interpretation we have calibrated the relationships between *net* rainfall, drip chemistry, and speleothem chemistry inside Hollow Ridge Cave (see Section 5.3). We demonstrated that: (1) increased *net* rainfall results in increased hydraulic loading, higher drip rates, and decreased water response times; (2) drip path length-dependent mixing between dissolved limestone and dissolved dolomite fixes initial dripwater Sr/Mg ratios at each site; (3) dripwater Sr/Ca and Mg/Ca ratios then evolve along PCP vectors away from the initial dripwater composition as a function of *net* rainfall (wet vs. dry); and (4) modern farmed calcite incorporates dripwater Sr/Mg ratios (Sr/Ca: Mg/Ca slopes on a PCP diagram) as a function of the ratio of distribution coefficients (D_{Sr}/D_{Mg}) (Fig. 6). These results suggest that under some conditions speleothems might faithfully archive *net* rainfall-driven variations in Mg/Ca and Sr/Ca ratios and provide valuable paleoclimate information. There are also conditions where it might *not* apply.

One implication of our analysis is that dripwater Sr/Ca vs. Mg/Ca ratios (Sr/Mg slope) must be more or less constant (constant bedrock-mixing ratio) in order to be diagnostic indicators of wet (less PCP) and dry periods (more PCP). This 'constant Sr/Mg ratio' is a first-order criterion for the interpretation of speleothem Mg/Ca and Sr/Ca time series: these two ratios must covary, and then must be in phase (constant Sr/Mg). Any period in a speleothem record where Sr/Ca and Mg/Ca do not covary coherently is likely due to variable bedrock-mixing (or some other process) and cannot be interpreted as simply wet versus dry.

Four high-quality speleothem Mg/Ca and Sr/Ca records are discussed here for illustration of Sr/Ca and Mg/Ca behavior (Fig. 8). Stalagmite HS-4 (Heshang Cave, China; Johnson et al., 2006) contains phase-locked Sr/Ca and Mg/Ca annual variations and constant Sr/Mg ratios in the youngest (top) 5000 μm ($R^2 = 0.55$) but this correlation disappears between 5000 and 6500 μm ($R^2 = 0.10$) (Fig. 8a). Stalagmite Bt2 (Botuverá Cave, Brazil; Cruz et al., 2007) contains highly coherent Mg/Ca and Sr/Ca record at millennial timescales and constant Sr/Mg ratios from present to 67 ka ($R^2 = 0.61$) and from 78 to 116 ka, but not between 68 and 78 ka ($R^2 = 0.04$) (Fig. 8b). Speleothem PN-95-5 (Père Noël Cave, Belgium; Verheyden et al., 2008) exhibits

extremely strong centennial correlation between Mg/Ca and Sr/Ca along the youngest 180 mm ($R^2 = 0.86$) and between 180 and 540 mm, but no correlation between 540 and 650 mm ($R^2 = 0.01$) (Fig. 8c).

Stalagmite "Big Guam" (Jinapsan Cave, Guam Island; Sinclair et al., 2012) is an example of how a long-term record of PCP can be overprinted by other processes such as variable bedrock-mixing (Fig. 8d). "Peak" Sr/Ca and Mg/Ca ratios (from 0 to 24 cm from tip) are broadly correlated ($R^2 = 0.55$), but several Mg/Ca increases (e.g., at 7 and 19 cm – arrows on Fig. 8d) are observed without corresponding Sr/Ca variation, suggesting that processes other than PCP (discussed below) controlled hydrochemistry during those intervals. "Plateau" Sr/Ca and Mg/Ca ratios are not correlated at all ($R^2 = 0.05$), suggesting that from 24 to 35 cm from the tip PCP had no effect on drip chemistry.

In summary, stalagmites HS-4, Bt2, PN-95-5, and Big Guam exhibit constant Sr/Mg ratios over centennial or millennial timescales suggesting that these stalagmites precipitated from drips with constant dissolved bedrock-mixing ratios and are good candidates for wet vs. dry paleohydrologic reconstruction. The Big Guam stalagmite exhibits non-constant Sr/Mg ratios over the "Plateau", thus it should not be considered a reliable archive of wet vs. dry paleohydrologic conditions during that time period. This criterion of near constant Sr/Mg might thus be a useful filter in applying paleohydrological interpretation to speleothem geochemical records. Several factors might lead to non-constant speleothem Sr/Mg ratios that would not support the PCP wet vs. dry interpretation, including: (1) changes in cave morphology, ventilation, and bedrock dripwater conduits and mixing; (2) non-constant formation temperature (Oomori et al., 1987; Huang and Fairchild, 2001); (3) large changes in growth rate (Baker et al., 1998; Banner et al., 2007; Tremaine et al., 2011) and crystallography (Lorens, 1978; Tesoriero and Pankow, 1996); (4) changes in mineralogy (Holland et al., 1963, 1964b); and (5) incongruent dissolution of host bedrock (McGillen and Fairchild, 2005).

Perhaps the most important application of these Sr/Mg criteria is that speleothem Mg/Ca and Sr/Ca records may offer insight into separating the 'amount effect' and 'source effect' in speleothem $\delta^{18}O$ records (Liu et al., 2013). Speleothem variations in $\delta^{18}O$ interpreted as monsoon-type 'amount effect' (Wang et al., 2008; Cheng et al., 2009) would require that higher Sr/Ca and Mg/Ca (dry; more PCP) should correlated with ^{18}O-enriched (heavier) calcite $\delta^{18}O$, and lower Sr/Ca and Mg/Ca ratios (wet; less PCP) should correlate with ^{18}O-depleted (lighter) calcite $\delta^{18}O$ in annually resolved records. Conversely, non-constant or incoherent speleothem Sr/Mg records that do not covary with variations in $\delta^{18}O$ are probably not a simple function of 'amount effect'.

7. CONCLUSIONS

High-resolution semi-continuous records of rainfall, drip rate, dripwater chemistry and seasonally farmed calcite chemistry at Hollow Ridge Cave have demonstrated that:

(1) Drip rate and water response time in the epikarst above HRC are controlled by *net* rainfall [P−ET]. Higher *net* rainfall results in increased drip rate and shorter drip rate response time to recharge (lag time). Drip rate response times are not synchronous throughout the cave.
(2) Dripwater SO_4/Cl and Na/Cl ratios behave quasi-conservatively in the epikarst, suggesting that they are suitable proxies for estimating evapotranspiration. Dripwater chloride, sodium, and sulfate concentrations are elevated ten to eighteen-fold above rainwater. Enrichments are weakly dependent on vertical drip path length and associated cumulative evapotranspiration effects.
(3) Dripwater [Mg^{2+}] and Mg/Ca ratios decrease with longer drip path lengths, while [Sr^{2+}] and Sr/Ca ratios increase. Both trends are due to dilution of dissolved high-Mg dolomitic caprock with dissolved low-Mg limestone as water chemistry evolves along the vertical drip paths.
(4) Dripwater hydrochemistry (Ca, Mg, Sr) in HRC and many other caves is best explained by two dominant mechanisms: (1) mixing between dissolved bedrock limestone and dissolved dolomite; and (2) Prior-Calcite-Precipitation driven evolution of dripwaters away from starting bedrock compositions toward higher Sr/Ca and Mg/Ca ratios.
(5) Variations in dripwater Sr/Ca and Mg/Ca ratios are preserved in contemporaneous speleothem calcite at sites with constant bedrock-mixing ratios – constant Sr/Mg. This calibration suggests that interpreting variations in speleothem Sr/Ca and Mg/Ca ratios as wet versus dry proxies require that the Sr/Mg ratio of speleothem calcite must be constant.
(6) Under constant speleothem Sr/Mg conditions, coherent and in-phase variations in speleothem $\delta^{18}O$, Sr/Ca and Mg/Ca may be confidently attributed to wet vs. dry rainfall *amount*.

ACKNOWLEDGMENTS

This research is conducted in conjunction with the Southeastern Cave Conservancy Inc. (SCCi), PO Box 71857, Chattanooga, TN 37407-0857, Director: K. Green with financial support from D. Baker, Plum Creek Timber, Seattle, WA. We thank A. Mosler, A. Kowalczk, B. Kilgore, S. Misra, and W. Landing for field support, sample collection, and method development. We thank D. Riechelmann, A. Baker, J. Baldini, J. Partin, C. Spötl, M. Musgrove, and I. Fairchild for providing unpublished drip chemistry data and F. Cruz, S. Verheyden, K. Johnson, and D. Sinclair for access to their high-resolution speleothem data sets. We thank W. Burnett, W. Landing, A. Ayalon, and two anonymous reviewers for refinement of previous drafts of this manuscript, as well as M. Bar-Matthews and F. McDermott for editorial handling. This work was funded by the Florida State University Francis Eppes Foundation and NSF Grant #AGS-1032403 to P.N.F., and by FSU-Oceanography teaching assistantships to D.T.

APPENDIX A. SUPPLEMENTARY DATA

Supplementary data associated with this article can be found, in the online version, at http://dx.doi.org/10.1016/j.gca.2013.07.026.

REFERENCES

Adams D. and Farwell S. (1981) Biogenic sulfur source strengths. *Eng. Sci. Technol.* **15**, 1493–1498.

Andreae M. (1990) Ocean-atmosphere interactions in the global biogeochemical sulfur cycle. *Mar. Chem.* **30**, 1–29.

Ayalon A., Bar-Matthews M. and Kaufman A. (1999) Petrography, strontium, barium and uranium concentrations, and strontium and uranium isotope ratios in speleothems as paleoclimatic proxies: Soreq Cave, Israel. *Holocene* **9**, 715–722.

Baker A., Smart P., Edwards R. and Richards D. (1993) Annual growth banding in a cave stalagmite. *Nature* **364**, 518–520.

Baker A., Barnes W. and Smart P. (1997) Variations in the discharge and organic matter content of stalagmite drip waters in Lower Cave, Bristol. *Hydrol. Process.* **11**, 1541–1555.

Baker A., Genty D., Dreybrodt W., Barnes W., Mockler N. and Grapes J. (1998) Testing theoretically predicted stalagmite growth rate with recent annually laminated samples: implications for past stalagmite deposition. *Geochim. Cosmochim. Acta* **62**, 393–404.

Baker A., Genty D. and Fairchild I. (2000) Hydrological characterisation of stalagmite dripwaters at Grotte de Villars, Dordogne, by the analysis of inorganic species and luminescent organic matter. *Hydrol. Earth Syst. Sci.* **4**, 439–449.

Baldini J., McDermott F. and Fairchild I. (2002) Structure of the 8200-year cold event revealed by a speleothem trace element record. *Science* **296**, 2203–2206.

Baldini J., McDermott F. and Fairchild I. (2006) Spatial variability in cave drip water hydrochemistry: implications for stalagmite paleoclimate records. *Chem. Geol.* **235**, 390–404.

Baldini J., McDermot F., Baldini L., Otley C., Linge K., Clipson B. and Jarvis K. (2012) Identifying short-term and seasonal trends in cave drip water trace element concentrations based on a daily-scale automatically collected drip water dataset. *Chem. Geol.* **330–331**, 1–16.

Banner J. (1995) Application of the isotope and trace element geochemistry of strontium to studies of diagenesis in carbonate systems. *Sedimentology* **42**, 805–824.

Banner J., Guilfoyle A., James E., Stern L. and Musgrove M. (2007) Seasonal variations in modern speleothem calcite growth in central Texas, U.S.A. *J. Sed. Res.* **77**, 615–622.

Bar-Matthews M., Ayalon A., Matthews A., Sass E. and Halicz L. (1996) Carbon and oxygen isotope study of the active water-carbonate system in a karstic Mediterranean cave: implications for paleoclimate research in semiarid regions. *Geochim. Cosmochim. Acta* **60**, 337–347.

Bar-Matthews M., Ayalon A., Kaufman A. and Wasserburg G. (1999) The Eastern Mediterranean paleoclimate as a reflection of regional events: Soreq cave, Israel. *Earth Planet. Sci. Lett.* **166**, 85–95.

Barnard W., Andreae M., Watkins W., Bingemer H. and Georgii H. (1982) The flux of dimethylsulfide from the oceans to the atmosphere. *J. Geophys. Res.* **87**(C11), 8787–8793.

Berner R. (1981) Kinetics of weathering and diagenesis. In *Kinetics of Geochemical Processes, Reviews in Mineralogy* (eds. A. C. Lasaga and R. S. Kirkpatrick). Mineral. Soc. Amer., Washington, DC, pp. 111–134.

Bidlake W., Woodham W. and Lopez M. (1996) Evapotranspiration from areas of native vegetation in west-central Florida. *U.S. Geol. Surv.*WATER-SUPPLY PAPER **2430**, 1–35.

Boch R., Spötl C. and Kramers J. (2009) High-resolution isotope records of early Holocene rapid climate change from two coeval stalagmites of Katerloch Cave, Austria. *Quat. Sci. Rev.* **28**, 2527–2538.

Borsato A., Frisia S., Fairchild I., Somogyi A. and Susini J. (2007) Trace element distribution in annual stalagmite laminae mapped by micrometer-resolution x-ray fluorescence: implications for incorporation of environmentally significant species. *Geochim. Cosmochim. Acta* **71**, 1494–1512.

Brezonik P., Edgerton E. and Hendry C. (1980) Acid precipitation and sulfate deposition in Florida. *Science* **208**, 1027–1029.

Broecker W., Olson E. and Orr P. (1960) Radiocarbon measurements and annual rings in cave formations. *Nature* **185**, 93–94.

Burns S., Fleitmann D., Matter A., Neff U. and Mangini A. (2001) Speleothem evidence from Oman for continental pluvial events during interglacial periods. *Geology* **29**, 623–626.

Busenberg E. and Plummer L. (1982) The kinetics of dissolution of dolomite in CO_2–H_2O systems at 1.5 to 60 degrees C and 0 to 1 atm PCO_2. *Am. J. Sci.* **282**, 45–78.

Chapman S. and Lindzen R. (1970). Atmospheric tides: thermal and gravitational. Dordrecht, Holland: D. Reidel Press, 200 pp.

Cheng H., Edwards R., Broecker W., Denton G., Kong X., Wang Y., Zhang R. and Wang X. (2009) Ice age terminations. *Science* **326**, 248–252.

Collister C. and Mattey D. (2005) High resolution measurement of water drip rates in caves using an accoustic drip counter. *EOS Trans. AGU*. **86**(52), Fall Meet. Suppl., Abstract PP31A–1496.

Cruz F., Burns S., Jercinovic M., Karmann I., Sharp W. and Vuille M. (2007) Evidence of rainfall variations in Southern Brazil from trace element ratios (Mg/Ca and Sr/Ca) in a Late Pliestocene stalagmite. *Geochim. Cosmochim. Acta* **71**, 2250–2263.

Dai A. and Wang J. (1999) Diurnal and semidiurnal tides in global surface pressure fields. *J. Atmos. Sci.* **56**, 3874–3891.

Day C. and Henderson G. (2011) Oxygen isotopes in calcite grown under cave-analogue conditions. *Geochim. Cosmochim. Acta* **75**, 3956–3972.

Desmarchelier J., Hellstrom J. and McCulloch M. (2006) Rapid trace element analysis of speleothems by ELA-ICP-MS. *Chem. Geol.* **231**, 102–117.

Fairchild I. and Baker A. (2012) *Speleothem Science: From Process to Past Environments*. Wiley Blackwell. ISBN: 978-4051-9620-8.

Fairchild I. and Treble P. (2009) Trace elements in speleothems as recorders of environmental change. *Quat. Sci. Rev.* **28**, 449–468.

Fairchild I., Killawee J., Sharp M., Spiro B., Hubbard B., Lorrain R. and Tison J. (1999) Solute generation and transfer from a chemically reactive alpine glacial-proglacial system. *Earth Surf. Proc. Land.* **24**, 1189–1211.

Fairchild I., Borsato A., Tooth A., Frisia S., Hawkesworth C., Huang Y., McDermott F. and Spiro B. (2000) Controls on trace element (Sr–Mg) compositions of carbonate cave waters: implications for speleothem climatic records. *Chem. Geol.* **166**, 255–269.

Fairchild I., Baker A., Borsato A., Frisia S., Hinton R., McDermott F. and Tooth A. (2001) Annual to sub-annual resolution of multiple trace-element trends in speleothems. *J. Geol. Soc.* **158**, 831–841.

Fairchild I., Tuckwell G., Baker A. and Tooth A. (2006) Modelling of dripwater hydrology and hydrogeochemistry in a weakly

karstified aquifer (Bath, UK): implications for climate change studies. *J. Hydrol.* **321**, 213–231.

Fairchild I., Spötl C., Frisia S., Borsato A., Susini J., Wynn P. and Cauzid J.EIMF (2010) Petrology and geochemistry of annually laminated stalagmites from an Alpine cave (Obir, Austria): seasonal cave physiology. *Geol. Soc. London Spec. Publ.* **336**, 295–321.

Finch A., Shaw P., Holmgren K. and Lee-Thorp J. (2003) Corroborated rainfall records from aragonitic stalagmites. *Earth Planet. Sci. Lett.* **215**, 265–273.

Frisia S., Borsato A., Fairchild I. and McDermott F. (2000) Calcite fabrics, growth mechanisms, and environments of formation in speleothems from the Italian Alps and Southwestern Ireland. *J. Sed. Res.* **70**, 1183–1196.

Gabitov R. and Watson E. (2006) Partitioning of strontium between calcite and fluid. *Geochem. Geophys. Geosyst.* **7**, 1–12.

Gascoyne M. (1983) Trace-element partition coefficients in the calcite-water system and their paleoclimatic significance in cave studies. *J. Hydrol.* **61**, 213–222.

Genty D. and Deflandre G. (1998) Drip flow variations under a stalactite of the Pere-Noel cave (Belgium). Evidence of seasonal variations and air pressure constraints. *J. Hydrol.* **211**, 208–232.

Goede A. and Vogel J. (1991) Trace element variations and dating of a late Pleistocene Tasmanian speleothem. *Palaeogeogr. Palaeoclimatol. Palaeoecol.* **88**, 121–131.

Goede A., McCulloch M., McDermott F. and Hawkesworth C. (1998) Aeolian contribution to strontium and strontium isotope variations in a Tasmanian speleothem. *Chem. Geol.* **149**, 37–50.

Green R., Evans III W., Bryan J. and Paul D. (2003) Geologic map of the eastern half of the U.S.G.S. 1:100,000 scale Marianna quadrangle, northwestern Florida. *USGS Open File Map Series 92-01*.

Griffiths M., Drysdale R., Gagan M., Frisia S., Zhao J., Ayliffe L., Hantoro W., Hellstrom J., Fischer M., Feng Y. and Suwargadi B. (2010) Evidence for Holocene changes in Australian-Indonesian monsoon rainfall from stalagmite trace element and stable isotope ratios. *Earth Planet. Sci. Lett.* **292**, 27–38.

Guilfoyle A. (2006) Temporal and spatial controls on cave water and speleothem calcite isotopic and elemental chemistry, Central Texas. Master's thesis, The University of Texas at Austin. p. 125.

Hellstrom J. and McCulloch M. (2000) Multi-proxy constraints on the climatic significance of trace element records from a New Zealand speleothem. *Earth Planet. Sci. Lett.* **179**, 287–297.

Henderson L. and Kraček F. (1927) The fractional precipitation of barium and radium chromates. *J. Am. Chem. Soc.* **49**, 739–749.

Hendy C. (1971) The isotopic geochemistry of speleothems. *Geochim. Cosmochim. Acta* **35**, 801–824.

Holland H., Borcsik M., Munoz J. and Oxburgh U. (1963) The coprecipitation of Sr^{+2} with aragonite and of Ca^{+2} with strontianite between 90 and 100 °C. *Geochim. Cosmochim. Acta* **27**, 957–977.

Holland H., Kirsipu T., Huebner J. and Oxburgh U. (1964a) On some aspects of the chemical evolution of cave waters. *J. Geol.* **72**, 36–67.

Holland H., Holland H. and Munoz J. (1964b) The coprecipitation of cations with $CaCO_3$ – II. The coprecipitation of S^{+2} with calcite between 90 ° and 100 °C. *Geochim. Cosmochim. Acta* **28**, 1287–1301.

Huang Y. and Fairchild I. (2001) Partitioning of Sr^{2+} and Mg^{2+} into calcite under karst-analogue experimental conditions. *Geochim. Cosmochim. Acta* **65**, 47–62.

Huang Y., Fairchild I., Borsato A., Frisia S., Cassidy N., McDermott F. and Hawkesworth C. (2001) Seasonal variations in Sr, Mg, and P in modern speleothems (Grotta di Ernesto, Italy). *Chem. Geol.* **175**, 429–448.

Ishikawa M. and Ichikuni M. (1984) Uptake of sodium and potassium by calcite. *Chem. Geol.* **42**, 137–146.

Jasechko S., Sharp Z., Gibson J., Birks S., Yi Y. and Fawcett P. (2013) Terrestrial water fluxes dominated by transpiration. *Nature* **496**, 347–350. http://dx.doi.org/10.1038/nature11983.

Jo K., Kyung S., Gi H., Kim S. and Suk B. (2010) Rainfall and hydrological controls on speleothem geochemistry during climatic events (droughts and typhoons): an example from Seopdong Cave, Republic of Korea. *Earth Planet. Sci. Lett.* **295**, 441–450.

Johnson K., Hu C., Belshaw N. and Henderson G. (2006) Seasonal trace-element and stable-isotope variations in a Chinese speleothem: the potential for high-resolution paleomonsoon reconstruction. *Earth Planet. Sci. Lett.* **244**, 394–407.

Karmann I., Cruz F., Viana O. and Burns S. (2007) Climate influence on geochemistry parameters of waters from Santana-Perolas cave system, Brazil. *Chem. Geol.* **244**, 232–247.

Katz A. (1973) The interaction of magnesium with calcite during crystal growth at 25–90 °C and one atmosphere. *Geochim. Cosmochim. Acta* **37**, 1563–1586.

Katz A., Sass E., Starinsky A. and Holland H. (1972) Strontium behavior in the aragonite-calcite transformation: an experimental study at 40–98 °C. *Geochim. Cosmochim. Acta* **36**, 481–496.

Kitano Y., Kanamori N. and Oomori T. (1971) Measurements of distribution coefficients of strontium and barium between carbonate precipitate and solution – abnormally high values of distribution coefficients measured at early stages of carbonate formation. *Geochem. J.* **4**, 183–206.

Kowalczk A. (2009) High resolution microclimate study of Hollow Ridge Cave: relationships between cave meteorology, air chemistry, and hydrology and the impact on speleothem deposition. Master's thesis, Florida State University, Department of Oceanography. Availabe from: <http://etd.lib.fsu.edu/theses/available/etd-10212009-010946/>.

Kowalczk A. and Froelich P. (2010) Cave air ventilation and CO_2 outgassing by radon-222 modeling: how fast do caves breathe?. *Earth Planet. Sci. Lett.* **289** 209–219.

Landing W., Caffrey J., Nolek S., Gosnell K. and Parker W. (2010) Atmospheric wet deposition of mercury and other trace elements in Pensacola, Florida. *Atmos. Chem. Phys.* **10**, 4867–4877.

Li H., Ku T., You C., Cheng H., Edwards R., Ma Z., Tsai W. and Li M. (2005) $^{87}Sr/^{86}Sr$ and Sr/Ca in speleothems for paleoclimate reconstruction in Central China between 70 and 280 kyr ago. *Geochim. Cosmochim. Acta* **69**, 3933–3947.

Likens G., Bormann F., Johnson N., Fisher D. and Pierce R. (1970) Effects of forest cutting and herbicide treatment on nutrient budgets in the Hubbard Brook watershed-ecosystem. *Ecol. Monogr.* **40**, 23–47.

Likens G., Driscoll C. and Buso D. (1996) Long-term effects of acid rain: response and recovery of a forest ecosystem. *Science* **272**, 244–246.

Liu Y.-H., Henderson G., Hu C.-Y., Mason A., Charnley N., Johnson K. and Xie S.-C. (2013) Links between the East Asian monsoon and the North Atlantic climate during the 8,200 year event. *Nat. Geosci.* **6**, 117–120.

Lorens R. (1978) A study of biological and physical controls on the trace metal content of calcite and aragonite. Ph. D. dissertation, University of Rhode Island.

Lorens R. (1981) Sr, Cd, Mn and Co distribution coefficients in calcite as a function of calcite precipitation rate. *Geochim. Cosmochim. Acta* **45**, 553–561.

Maddox G. (1993) Karst features of Florida Caverns State Park and falling waters state recreation area: Jackson and Washington Counties, Florida. *Southeastern Geological Survey*, Tallahassee, FL.

McDonald J. and Drysdale R. (2004) The 2002–2003 El Nino recorded in Australian cave drip waters: implications for reconstructing rainfall histories using stalagmites. *Geophys. Res. Lett.* **31**, L22202, 22201–22204.

McDonald J., Drysdale R., Hill D., Chisari R. and Wong H. (2007) The hydrochemical response of cave drip waters to sub-annual and inter-annual climate variability, Wombeyan Caves, SE Australia. *Chem. Geol.* **244**, 605–623.

McGillen M. and Fairchild I. (2005) An experimental study of incongruent dissolution of $CaCO_3$ under analogue glacial conditions. *J. Glaciol.* **51**, 383–390.

McIntire W. (1963) Trace element partition coefficients – a review of theory and applications to geology. *Geochim. Cosmochim. Acta* **27**, 1209–1264.

McMillan E., Fairchild I., Frisia S., Borsato A. and McDermott F. (2005) Annual trace element cycles in calcite-aragonite speleothems: evidence of drought in the western Mediterranean 1200–1100 yr BP. *J. Quat. Sci.* **20**, 423–433.

Mickler P., Banner J., Stern L., Asmerom Y., Edwards R. and Ito E. (2004) Stable isotope variations in modern tropical speleothems: evaluating equilibrium vs. kinetic isotope effects. *Geochim. Cosmochim. Acta* **68**, 4381–4393.

Mickler P., Stern L. and Banner J. (2006) Large kinetic isotope effects in modern speleothems. *Geol. Soc. Am. Bull.* **118**, 65–81.

Morse J. (2003) 7.03 – Formation and diagenesis of carbonate sediments. In *Treatise on Geochemistry* (eds. H. Holland, K. Turekian), *Elsevier*, pp. 3533–3551.

Morse J. and Bender M. (1990) Partitioning coefficients in calcite: examination of factors influencing the validity of experimental results and their application to natural systems. *Chem. Geol.* **82**, 265–277.

Mucci A. and Morse J. (1983) The incorporation of Mg^{2+} and Sr^{2+} into calcite overgrowths: influences of growth rate and solution composition. *Geochim. Cosmochim. Acta* **47**, 217–233.

Mucci A. and Morse J. (1990) Chemistry of low-temperature abiotic calcites: experimental studies on coprecipitation, stability and fractionation. *Rev. Aquat. Sci.* **3**, 217–254.

Münsterer C., Fohlmeister J., Christl M., Shröder-Ritzrau A., Alfimov V., Ivy-Ochs S., Wackerbarth A. and Mangini A. (2012) Cosmogenic ^{36}Cl in karst waters from Bunker Cave North Western Germany – a tool to derive location evapotranspiration? *Geochim. Cosmochim. Acta* **86**, 138–149.

Musgrove M. and Banner J. (2004) Controls on the spatial and temporal variability of vadose dripwater geochemistry: Edwards Aquifer, central Texas. *Geochim. Cosmochim. Acta* **68**, 1007–1020.

Okumura M. and Kitano Y. (1986) Coprecipitation of alkali metal ions with calcium carbonate. *Geochim. Cosmochim. Acta* **50**, 49–58.

Oomori T., Kaneshima H., Maezato Y. and Kitano Y. (1987) Distribution coefficient of Mg^{2+} ions between calcite and solution at 10–50 °C. *Mar. Chem.* **20**, 327–336.

Oster J., Montanez I. and Kelley N. (2012) Response of a modern cave system to large seasonal precipitation variability. *Geochim. Cosmochim. Acta* **91**, 92–108.

Palmer M. R. and Edmond J. M. (1992) Controls over the strontium isotope composition of river water. *Geochim. Cosmochim. Acta* **56**, 2099–2111.

Partin J., Jenson J., Banner J., Quin T., Taylor F., Sinclair D., Hardt B., Lender M., Bell T., Miklavic B., Jocson J. and Taborosi D. (2012) Relationship between modern rainfall variability, cave dripwater and stalagmite geochemistry in Guam, USA. *Geochem. Geophys. Geosyst.* **13**, Q03013. http://dx.doi.org/10.1029/2011GC003930.

Parungo F., Nagamoto C., Hoyt S. and Bravo A. (1990) The investigation of air quality and acid rain over the Gulf of Mexico. *Atmos. Environ. A Gen. Top.* **24**, 109–123.

Pilson M. (1998) *An Introduction to the Chemistry of the Sea*, first ed. Prentice Hall.

Pingitore N. and Eastman M. (1984) The experimental partitioning of Ba^{2+} into calcite. *Chem. Geol.* **45**, 113–120.

Pingitore N. and Eastman M. (1986) The coprecipitation of Sr^{2+} with calcite at 25 degrees C and 1 atm. *Geochim. Cosmochim. Acta* **50**, 2195–2203.

Polyak V. and Asmerom Y. (2001) Late Holocene climate and cultural changes in the southwestern United States. *Science* **294**, 148–151.

Riechelmann D., Schroder-Ritzrau A., Scholz D., Fohlmeister J., Spötl C., Richter D. and Mangini A. (2011) Monitoring Bunker Cave (NW Germany): a prerequisite to interpret geochemical proxy data of speleothems from this site. *J. Hydrol.* **409**, 682–695.

Roberts M., Smart P. and Baker A. (1998) Annual trace element variations in a Holocene speleothem. *Earth Planet. Sci. Lett.* **154**, 237–246.

Roberts M., Smart P., Hawkesworth C., Perkins W. and Pearce N. (1999) Trace element variations in coeval Holocene speleothems from GB Cave, southwest England. *Holocene* **9**, 707–713.

Scott T. (1991) A geological overview of Florida. In: *Florida's Ground Water Quality Monitoring Program – Hydrogeologic Framework* (eds. T. Scott, J. Lloyd, G. Maddox). Florida Geological Survey Special Publication 32, Tallahassee, FL. pp. 97.

Scott T. (2001) *Geologic Map of the State of Florida and Open File Report 80*. Florida Geological Survey, United States Geological Survey, Tallahassee, FL. p. 30.

Sherwin C. and Baldini J. (2011) Cave air and hydrological controls on prior calcite precipitation and stalagmite growth rates: implications for paleoclimate reconstructions using speleothems. *Geochim. Cosmochim. Acta* **75**, 3915–3929.

Sinclair D., Banner J., Taylor F., Partin J., Jenson J., Mylroie J., Goddard E., Quinn T., Jocson J. and Miklavic B. (2012) Magnesium and strontium systematics in tropical speleothems from the Western Pacific. *Chem. Geol.* **294–295**, 1–17.

Smart P. and Friedrich H. (1986) Water movement and storage in the unsaturated zone of a maturely karstified carbonate aquifer. In *Proc. Conf. on Environmental Problems of Karst Terrains and Their Solution*, Mendip Hills, England. pp. 57–87.

Smith C., Fairchild I., Spötl C., Frisia S., Borsato A., Moreton S. and Wynn P. (2009) Chronology building using objective identification of annual signals in trace element profiles of stalagmites. *Quatern. Geochronol.* **4**, 11–21.

Spötl C., Fairchild I. and Tooth A. (2005) Cave air control on dripwater geochemistry, Obir Caves (Austria): implications for speleothem deposition in dynamically ventilated caves. *Geochim. Cosmochim. Acta* **69**, 2451–2468.

Stallard R. and Edmond J. (1983) Geochemistry of the Amazon 2. The influence of geology and weathering environment on the dissolved load. *J. Geophys. Res.* **88**, 9671–9688.

Stern L., Banner J., Cowan B., Copeland E., Mickler P., Guilfoyle A., James E., Musgrove M. and Mack L. (2005) Trace element variations in speleothem calcite: influence of non-environmental factors. *Geol. Soc. Am. Abstr. Prog.* **193**, 435.

Tesoriero A. and Pankow J. (1996) Solid solution partitioning of Sr^{2+}, Ba^{2+}, and Cd^{2+} to calcite. *Geochim. Cosmochim. Acta* **60**, 1053–1063.

Tooth A. and Fairchild I. (2003) Soil and karst aquifer hydrological controls on the geochemical evolution of speleothem-forming drip waters, Crag Cave, southwest Ireland. *J. Hydrol.* **273**, 51–68.

Treble P., Shelley J. and Chappell J. (2003) Comparison of high resolution sub-annual records of trace elements in a modern (1911–1992) speleothem with instrumental climate data from southwest Australia. *Earth Planet. Sci. Lett.* **216**, 141–153.

Treble P., Chappell J. and Shelley J. (2005) Complex speleothem growth processes revealed by trace element mapping and scanning electron microscopy of annual layers. *Geochim. Cosmochim. Acta* **69**, 4855–4863.

Tremaine D. (2010) Speleothem paleoclimatology and modern speleochemistry proxies: calcite farming in a continuously monitored cave. Master's thesis, Florida State University. Available from: <http://etd.lib.fsu.edu/theses/available/etd-07052010-230757/>.

Tremaine D., Froelich P. and Wang Y. (2011) Speleothem calcite farmed *in situ*; modern calibration of $\delta^{18}O$ and $\delta^{13}C$ paleoclimate proxies in a continuously-monitored natural cave system. *Geochim. Cosmochim. Acta* **75**, 4929–4950.

Verheyden S., Keppens E., Fairchild I., McDermott F. and Weis D. (2000) Mg, Sr, and Sr isotope geochemistry of a Belgian Holocene speleothem: implications for paleoclimate reconstructions. *Chem. Geol.* **169**, 131–144.

Verheyden S., Genty D., Deflandre G., Quinif Y. and Keppens E. (2008) Monitoring climatological, hydrological and geochemical parameters in the Père Noël cave (Belgium): implication for the interpretation of speleothem isotopic and geochemical time-series. *Int. J. Speleol.* **37**, 221–234.

Wang Y., Cheng H., Edwards R., Kong X., Shao X., Chen S., Wu J., Jiang X., Wang X. and An Z. (2008) Millenial- and orbital-scale changes in the East Asian monsoon of the past 224,000 years. *Nature* **451**, 1090–1093.

Williams D., Cable W., Hultine K., Hoedjes J., Yepez E., Simonneaux V., Er-Raki S., Boulet G., de Bruin H., Chehbouni A., Hartogensis O. and Timouk F. (2004) Evapotranspiration components determined by stable isotope, sap flow and eddy covariance techniques. *Agric. For. Meteorol.* **125**, 241–258.

Willmot C., Rowe C. and Mintz Y. (1985) Climatology of the terrestrial seasonal water cycle. *J. Climatol.* **5**, 589–606.

Wong C., Banner J. and Musgrove M. (2011) Seasonal dripwater Mg/Ca and Sr/Ca variations driven by cave ventilation: implications for and modeling of speleothem paleoclimate records. *Geochim. Cosmochim. Acta* **75**, 3514–3529.

Yu J., Day J., Greaves M. and Elderfield H. (2005) Determination of multiple element/calcium ratios in foraminiferal calcite by quadrupole ICP-MS. *Geochem. Geophys. Geosyst.* **6**, 9.

Zhong S. and Mucci A. (1995) Partitioning of rare earth elements (REEs) between calcite and seawater solutions at 25 °C and 1 atm, and high dissolved REE concentrations. *Geochim. Cosmochim. Acta* **59**, 443–453.

Associate editor: F. McDermott